A Statistical Approach for Characterizing the Behaviour of Roughness Parameters Measured by a Multi-Physics Instrument on Ground Surface Topographies: Four Novel Indicators

Clément Moreau [1,2], Julie Lemesle [3,4], David Páez Margarit [5], François Blateyron [2] and Maxence Bigerelle [1,*]

[1] Univ. Polytechnique Hauts-de-France, CNRS UMR 8201—LAMIH—Laboratoire d'Automatique, de Mécanique et d'Informatique Industrielles et Humaines, F–59313 Valenciennes, France; clementmoreau.etudes@gmail.com

[2] Digital Surf, 25000 Besançon, France; fblateyron@digitalsurf.fr

[3] Valutec, Univ. Polytechnique Hauts-de-France, 59314 Valenciennes, CEDEX 9, France; julie.lemesle@uphf.fr

[4] U.R Concept, 59300 Valenciennes, France

[5] Sensofar Metrology, 08225 Terrassa, Barcelona, Spain; paez@sensofar.com

* Correspondence: maxence.bigerelle@uphf.fr

Abstract: With a view to improve measurements, this paper presents a statistical approach for characterizing the behaviour of roughness parameters based on measurements performed on ground surface topographies (grit #080/#120). A S neox^{TM} (Sensofar$^®$, Terrassa, Spain), equipped with three optical instrument modes (Focus Variation (FV), Coherence Scanning Interferometry (CSI), and Confocal Microscopy (CM)), is used according to a specific measurement plan, called Morphomeca Monitoring, including topography representativeness and several time-based measurements. Previously applied to the Sa parameter, the statistical approach based here solely on the Quality Index (*QI*) has now been extended to a multi-parameter approach. Firstly, the study focuses on detecting and explaining parameter disturbances in raw data by identifying and quantifying outliers of the parameter's values, as a new first indicator. This allows us to draw parallels between these outliers and the surface topography, providing reflection tracks. Secondly, the statistical approach is applied to highlight disturbed parameters concerning the instrument mode used and the concerned grit level with two other indicators computed from *QI*, named homogeneity and number of modes. The applied method shows that a cleaning of the data containing the parameters values is necessary to remove outlier values, and a set of roughness parameters could be determined according to the assessment of the indicators. The final aim is to provide a set of parameters which best describe the measurement conditions based on monitoring data, statistical indexes, and surface topographies. It is shown that the parameters Sal, Sz and Sci are the most reliable roughness parameters, unlike Sdq and S5p, which appear as the most unstable parameters. More globally, the volume roughness parameters appear as the most stable, differing from the form parameters. This investigated point of view offers thus a complementary framework for improving measurement processes. In addition, this method aims to provide a global and more generalizable alternative than traditional methods of uncertainty calculation, based on a thorough analysis of multi-parameter and statistical indexes.

Keywords: roughness parameter family; focus variation; confocal microscope; coherence scanning interferometer; uncertainty; reliability

1. Introduction

As geologists study the terrain relief [1], surface topography investigators aim to understand the history of the surface [2], but physical phenomena at different scales [3,4] could be linked (scale continuity), as in [5]. Particularly in tribology, understanding physical phenomena is necessary to functionalize surface topography in order to tune the behaviour of a final product, according to its use [6–9]. These tribological phenomena occur at the

interface between two topographical features in contact and moving relative to each other. This is why it is necessary to analyse the topography of these surfaces, because they play a crucial role in how these phenomena manifest, and thus they are key to explaining them. Among these tribological phenomena, there are friction [10], wear [11], which results from the progressive deterioration of surfaces caused by friction, lubrication [12], which tends to modify the friction conditions and avoid premature wear, adhesion [13], which is an attractive force which contributes to friction conditions, contact fatigue [14], and even tribo-corrosion [15]. Understanding these tribological phenomena through surfaces topographies significantly contributes to various fields, including materials engineering [5] and mechanical systems design [16,17].

There exist two types of instruments for measuring surface topographies: tactile and optical. Tactile profilometry stands as one of the most commonly utilized techniques for surface metrology in both research and industry, but this measurement technic is, little by little, being replaced by the optical profilometers. The advantages of the optical profilometers are their ability to carry out quick 3D measurements with different technologies, such as Focus Variation [18,19], Confocal Microscopy [20] and Interferometry [21,22]. The diversity of optical instruments allows us to choose the most adequate technology regarding the features of the measured surface (form, slope, brightness, smoothness, etc.). However, depending on the characteristics of the surface, measurement uncertainties can occur, especially with optical instruments. The instrument choice could be thus determined by its ability to measure a given surface landscape regarding the generated uncertainties (as defined in [23]).

Choosing an adequate instrument with its significant settings [24,25] is not the only problematic factor in metrology. It is necessary to perform a judicious image treatment [26,27] to put forward the required information, and then describe the surface topographies with roughness parameters. A question could arise: what is a good parameter and how can we determine its reliability for the carried-out measurement campaign?

1.1. State of the Art

1.1.1. Sources of Roughness Parameter Fluctuations

The roughness parameters are indicators that can describe a range of features such as characteristic heights, height distribution maps (based on the Abbott–Firestone curve), periodicity, directionality of textures, local gradients, fractal aspects, volume characteristics, and surface topography motifs. These various types of parameters can also be influenced by numerous factors, including the instrument used to perform the measurement, the inherent properties of the surface, the measurement plan (such as repositioning and the duration of acquisition), and uncertainties (such as environmental disturbances or instrument drift).

Surface/Instrument Interaction

In the field of this study, a Sensofar S neox (Sensofar®, Terrassa, Spain) device is used. This device includes three types of instruments: Coherence Scanning Interferometry (CSI), 3D field Confocal Microscope (CM) and Focus Variation or Shape-from-Focus (FV). Regarding the state of the art, only these instruments are taken into account. In this part, the focus is on the interaction between instruments and intrinsic properties of the surface. Sometimes, no reference is found, due to the incompatibility of the measuring conditions and the instruments.

The studied surface landscape type determines the entire investigation process. Indeed, the optical and geometrical properties of a physical specimen play a main role regarding the most adequate instrument and its ability to measure, more especially the interaction between the surface and the instrument. These intrinsic properties are described in Appendix A and are faced regarding the instrument type defined before, to highlight if an instrument is commonly used regarding a given property (optical or geometrical).

Measurement Conditions

The specimen repositioning is the major source of topographical variations in metrology, whether repositioning is carried out manually or by a displacement table [28]. This is why a measurement plan including multiple measurements at a given position reproduced at multiple positions could impact the results. But the instrument settings used to perform the measurement campaign have an impact too. The magnification, the lateral resolution [29], the scanning speed [30], the type and the intensity of light source [31] are some examples of a non-exhaustive list of major instrument settings which have a crucial impact.

Environment

Instruments can face external fluctuations such as temperature, light, the hygrometry or human activities. These aspects of fluctuation depend on the place when the instrument is installed. Some preconisation is explained by the VDI/VDE 2655 [32]. These evolutions could be followed during the measuring time with sensors such as a vibrometer, a anemometer, or others, in order to try to describe more precisely the impact of the environment on the measurements.

1.2. Uncertainty Determination

1.2.1. Classical Methods

In surface metrology, uncertainty is a complex and critical issue, influenced by various factors and requiring rigorous methodological approaches for a precise evaluation. Among the methods used to quantify these uncertainties, the *Guide to the Expression of Uncertainty in Measurement (GUM)* [33] provides a standardized framework based on the propagation of uncertainties. The Monte Carlo method, recommended by the *Supplement 1* of GUM [34], allows for the simulation and assessment of the impact of uncertainties by generating probability distributions for the measured variables, thus providing a robust estimation of combined uncertainties.

The uncertainties calculated with direct methods are obtained by comparison of the signal obtained by the instrument with the theorical signal, while the uncertainties calculated with indirect methods are obtained by subtraction. Substitution is a commonly used technique where the direct measurement is replaced by an indirect measurement of a known quantity, facilitating the evaluation of uncertainties [35,36] when direct measurement is difficult or impossible. The uncertainties are composed of many sources of fluctuation, such as the measurement noise generated by speckle fluctuations in White Light Interferometry (WLI) [37–39], and are calculated from intensity. It is essential to account for this noise, as well as other deviations such as flatness correction [40] or lateral resolution [29] and the Z-axis scale [41], to ensure the reliability of measurements.

Intercomparison of instruments, based on statistical methods, is necessary to evaluate the influence of each instrument on the measurement. This includes comparisons of optical profilometers, where the results from different instruments must be equivalent in accordance with filtering and lateral-resolution standards. However, it is crucial to consider the specific metrological characteristics of each instrument as defined by ISO 25178-6 [42] and ISO 25178-60X [43–48] standards, as well as to calibrate and verify these instruments to correctly assess uncertainties, particularly by using recommended good practice guides.

Due to the complexity of applying classical methods for determining uncertainties on real surfaces and estimating these uncertainties across all roughness parameters, alternative methods have been developed.

1.2.2. Unconventional Methods

(X, Y) Method

A method based on gradients and height standard deviation of surface topography pixels was developed to study measurement fluctuations [49,50]. This method quantifies uncertainties from repeated measurements at the same position and links them to surface gradients through a visual tool, B^{2}D plots in 2D and 3D. As a result, height fluctuations

(standard deviation) are correlated to gradients, and the height fluctuations depend on both abrasion level and light/sub-layer interaction for the abraded lens.

Allan Deviation

Surface uncertainty assessment using Allan deviation [51] reveals the limitations of traditional methods. Two types of Allan deviation can be calculated for surface topography series: lateral and temporal deviation, both based on Sq^2. The lateral deviation describes the variation in Z (X, Y) using the root mean square of Sq between each map and the mean map of a given series. In contrast, the temporal deviation accounts for multiple subsets of long-term measurement series and includes a mean filter to describe a time trend. Unlike ISO 25178-600 [35] and ISO 25178-700 [36] standards that assume stationary and randomly distributed noise, the Allan deviation shows that these assumptions do not always hold. The temporal Allan deviation indicates that averaging over longer periods may not improve mean values if drifts or spikes occur. The lateral Allan deviation reveals implicit or explicit filtering, often unnoticed in classical analyses, affecting the lateral resolution. These methods enable in-depth analysis of non-stationary noise and lateral correlations, providing a detailed understanding of uncertainties in surface measurements.

Coefficient Determination Method

Another method allowing us to follow the measurement deviation is presented in [52,53], using S neox^{TM} (Sensofar$^{®}$, Terrassa, Spain), and shows several important findings in real-world conditions. The method is based on the determination coefficient R^2 and shows the Z (X, Y) fluctuations between two measurements or a data set, allowing us to compare different configurations. This method can be used to show the time evolution of height regarding the time or the difference of height obtained with two different measurement modes. It allows us to quickly assess the repeatability, precision, and uncertainty of topographic measurements. Each height value from the maps is plotted on a 2D chart, with the height of the nth map as the X coordinate and the height of the (n + 1)th map as the Y coordinate, allowing us to compute the R^2 coefficient. It also determines how consistent the measurements are between different optical modes. Measurements with the same mode show very low height variations and a strong coefficient (R^2 > 0.99). However, measurements between different modes correlate less (R$^2 \approx 0.88$), and display different slopes on their height–height plots. Overall, this assessment method shows the Confocal mode is the most repeatable, with the strongest correlations, and tends to measure slightly higher heights compared to the other modes. The method efficiently estimates measurement reliability and noise levels, crucial for evaluating topographic data accuracy.

Index Method

Finally, the method developed in [54] shows statistical indicators developed to discriminate two surfaces with neighbouring roughness, while considering stability, drift, and signal-to-noise ratio, in order to help improve the quality of measurements. Unlike the precedent approach, the developed indexes are computed from roughness parameters calculated on the height maps, and not directly from the height maps. By using these indexes, it is possible to determine if an instrument can effectively distinguish two similar surfaces, to evaluate the impact of the stitching process (combining measurements) on data quality [55], and thus to enhance the precision and relevance of measurements in surface topography studies.

More globally, absolute metrology refers to the precise and unbiased measurement of surfaces, aiming to provide results that are not influenced by the calibration of instruments based on standardized specimens. However, the challenge arises when the real-world surfaces differ from these standardized specimens, leading to instrument bias. Additionally, roughness parameters, typically developed for simplified surfaces, may not accurately represent real surfaces, creating a bias in the measurement results. Uncertainties in this context are also problematic, as they stem from various sources, including environmental

factors and instrument limitations, making it difficult to quantify them accurately. To address these challenges and to be independent of the device set-up, relative metrology steps in, focusing on the comparison of surfaces (A/B), considering roughness parameters, scale, and process conditions. A well-structured measurement plan can help validate parameters and control uncertainties, ensuring better quality, stability, and relevance in measurements.

1.2.3. Uncertainty Methods Comparison

Table 1 presents a comparison of the conventional and unconventional methods for estimating measurement uncertainties.

Table 1. Summary of uncertainty calculation methods, showing their respective strengths and weaknesses.

Uncertainty Method	Strengths	Weaknesses
GUM/ISO	• Approved by the ISO committee and supported by most metrologists • Established for standard surfaces • Takes into account multiple sources of uncertainties	• Difficult to apply to real surfaces • Time effect not taken into account • Could be difficult to implement for non-linear effects • Time consuming
X, Y mapping	• Mapping visualisation and correlation with the surface gradients	• Sensitive to specimen drift • Depends on the number and frequency of map acquisitions
Allan deviation (lateral and temporal)	• Time effect taken into account • Non-stationary noise detected (drift, spikes, modulation or regime changes)	• Method more difficult to implement than ISO 25478-600/700 [35,36] • Noise distribution is not clearly Gaussian, making it difficult to model
Correlation	• Easy to implement • Trend modelling is straightforward	• Uncertainty quantification is not direct • Height sensitivity to outliers' map values
Statistical index	• Allows for the clear assessment of the instruments' performances • Includes four type of indicators which are complementary • Adapted to real surfaces and comparisons	• Can be difficult to implement directly • Statistical knowledge required • Roughness parameter selection is not direct in assessment of the instrument performance

1.3. Objectives

The primary objective of this paper is to develop a methodology based on a statistical index (here the Quality Index) for identifying reliable roughness parameters coming from a given surface topography (surface #080/#120) and the instruments used (S neox^{TM} Sensofar$^{®}$, Terrassa, Spain), including Focus Variation, Confocal and Interferometry profilometers). This involves evaluating parameters both through direct raw data analysis and a developed statistical index (Quality Index). An important aspect of this study is to identify the best and worst parameters which highlight measurement problems, and to study the worst parameters to know if they can be valuable indicators.

To achieve this, four novel indicators were developed based on the Quality Index (*QI*): the percentage of outliers of the roughness parameter values, the number of modes, and the homogeneity of *QI*. The percentage of outliers is calculated from the raw data to identify values that deviate from the main population. Subsequently, the *QI* is applied to each roughness parameter, grit level, and measurement mode. This process allows for the computation of two additional indicators based on the *QI* distribution: the number of modes in the *QI* distribution and the homogeneity which reflects the ability to fit the *QI* distribution using unimodal and polymorphic modelling. The goal is to assess whether measurement conditions (such as measurement plans and instrument modes) or the level

of surface grinding influence the quality index through a comparative assessment of these indicators.

This methodology aims to identify reliable parameters and explain discrepancies through topographical analysis. It includes comparing the raw data approach with statistical index analysis to decide if the outliers of the roughness parameter values should be removed from the database, and validating the results with statistical indexes. Finally, we will discuss how this new methodology could replace or complement existing uncertainty calculation methods, which are often limited to specific cases, thus providing a more generalized approach.

2. Materials and Methods

2.1. Surface Description

The TA6V material was selected for its ability to maintain surface conditions. Two TA6V rods, of 10 mm thickness and 30 mm diameter, were cut using a machine with a diamond cutting disc, and pre-ground with a Silicon Carbide (SiC) grinding paper P#320 to remove cutting scratches and residual stresses. They were then ground with SiC papers from grit P#80 to grit P#1200 for 2 min each, at 300 rpm, with a normal force of 30 N. Finally, one specimen was ground with P#80 (called #080) and the other with P#120 (called #120) for 15 min, at 300 rpm, with a normal force of 30 N, using water lubrication. The surface mechanisms are described in Appendix B.

2.2. Measurement Description

2.2.1. Instrument Settings

The S neox^{TM} (Sensofar$^®$, Terrassa, Spain) 3D optical profilometer was chosen to carry out the measurement campaign, supporting Focus Variation (FV), Confocal Microscopy (CM), and Coherence Scanning Interferometry (CSI). The FV and CM modes used a green LED light source and a 20× EPI Nikon lens, while the CSI mode employed a white LED light source and a 20× DI Mirau lens. The system featured a 1.2-megapixel camera with a pixel size of 0.69 μm, offering Z-scaling [56] of 8 nm for continuous CM and FV modes, and 1 nm for CSI mode. The vertical scan range was configured to 128 μm for FV and CM modes, and 30 μm for CSI mode.

2.2.2. Measurement Strategy

A dedicated measurement plan was used to perform measurements [54]. The measurement process was automated. This measurement plan included a multi-measurement strategy: 30 zones per specimen (30 repetitions) and 10 iterations at each given location. The zones were randomly determined at the beginning of the measurement process, then set for the entirety of the study and for the three instrument modes. Each measurement lasted between 1 and 3 s. Each measurement presented raw data without any post-processing. The measurements were of the elementary surfaces, avoiding stitching, and thus ensuring detailed topographies sufficient for statistically robust roughness-parameter calculations.

Figure 1 shows the measurement order according to the two grit levels (in green), the three instrument modes (in red), the repetitions (in blue) and the iterations (in black). For instance, during 1 iteration step, 30 repetitions are performed, and 60 grit alternations are made.

Figure 2 allows for the illustration of the measurement process according to the repetitions, the iterations and the alternance between the grit levels. It is specified that the grit level alternance is made at each measurement. The repetitions are incremented at each position on a given specimen, as shown in Figure 2. After measuring all measurement repetitions, i.e., all positions on the surface, a new measurement cycle is performed, corresponding to the iteration step. This measurement process is carried out for all instrument modes without removing the specimen, to measure the same area and to have comparative measurements.
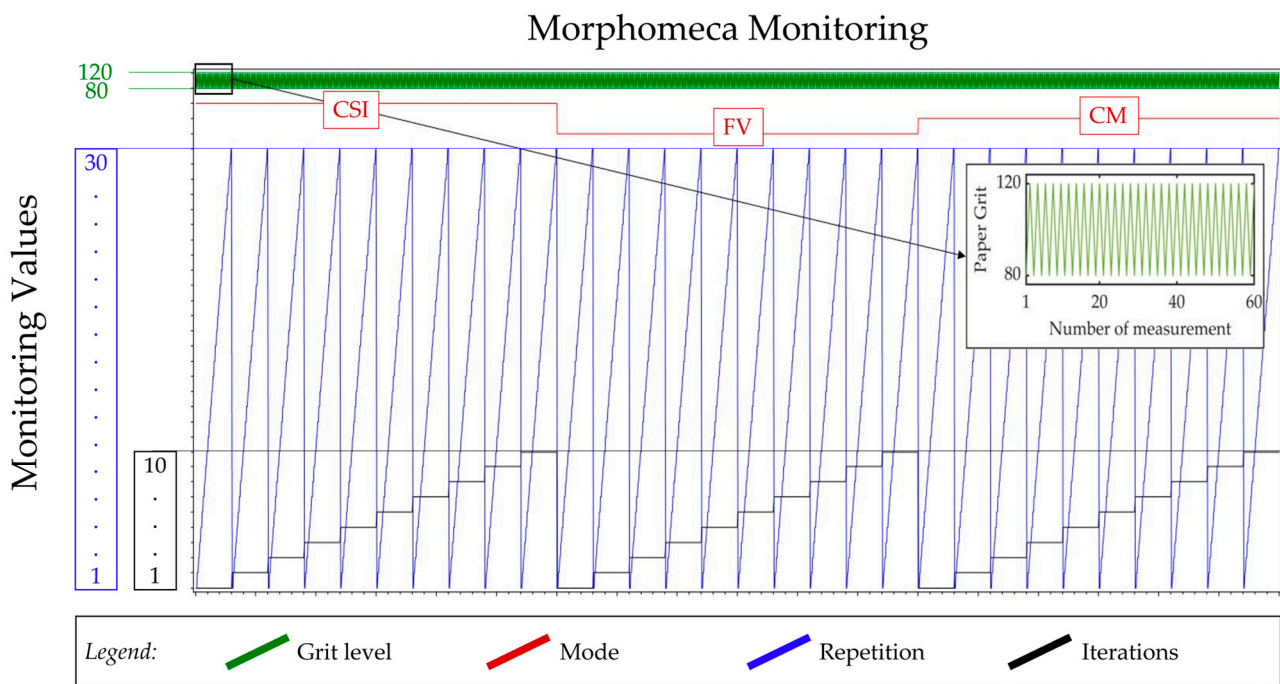
Figure 1. Morphomeca Monitoring showing the measurement strategy according to the paper grit levels, the measurement modes, the iterations, and the repetitions [54].
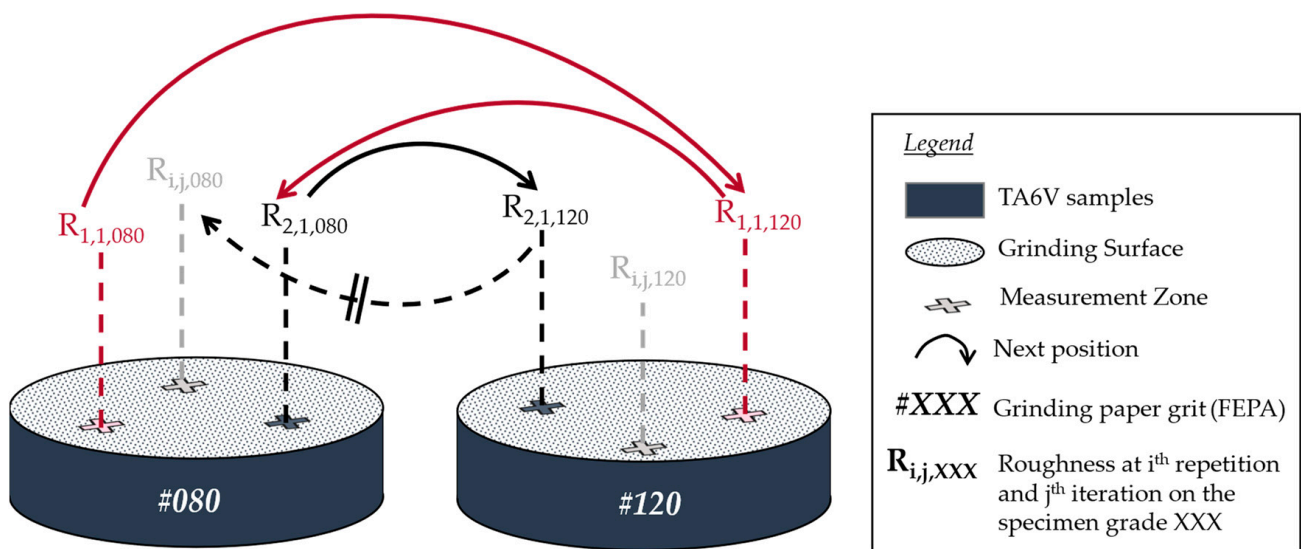

Figure 2. Scheme of measurement process steps [54].

2.3. Data Post-Processing

2.3.1. Topography Processing

The surface post-processing, performed with MountainsMap®, is simplified to facilitate direct comparison of measurements, without the need for operator intervention to clean the surface. Figure 3 illustrates the difference in roughness parameter calculation between a raw surface and a surface where a second-order removal form was applied. Removing the form significantly influences the results, highlighting the necessity of this step in our case. No S-filter or C-filter was applied to the surface topographies, to ensure that the comparison remains unaffected by image processing.
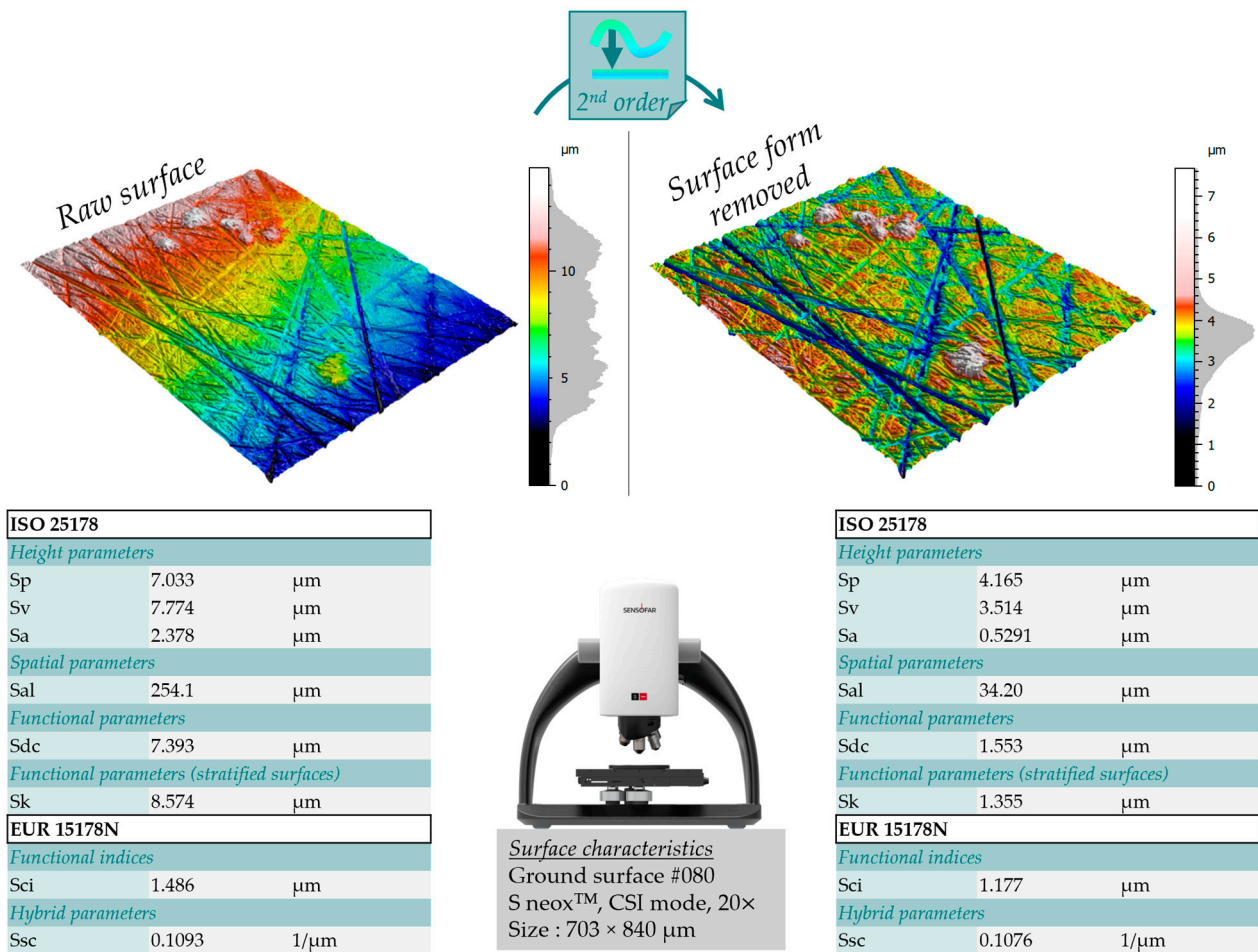
ISO 25178		
Height parameters		
Sp	7.033	µm
Sv	7.774	µm
Sa	2.378	µm
Spatial parameters		
Sal	254.1	µm
Functional parameters		
Sdc	7.393	µm
Functional parameters (stratified surfaces)		
Sk	8.574	µm
EUR 15178N		
Functional indices		
Sci	1.486	µm
Hybrid parameters		
Ssc	0.1093	1/µm

Surface characteristics
Ground surface #080
S neox™, CSI mode, 20×
Size : 703 × 840 µm

ISO 25178		
Height parameters		
Sp	4.165	µm
Sv	3.514	µm
Sa	0.5291	µm
Spatial parameters		
Sal	34.20	µm
Functional parameters		
Sdc	1.553	µm
Functional parameters (stratified surfaces)		
Sk	1.355	µm
EUR 15178N		
Functional indices		
Sci	1.177	µm
Hybrid parameters		
Ssc	0.1076	1/µm

Figure 3. Example of a ground surface with and without a second-order form removal, and calculation of some roughness parameters.

2.3.2. Index Computation

To simplify the analysis and avoid working directly on the raw data of roughness parameters, a series of statistical indexes was developed [54]. In this publication, only the Quality Index (*QI*) is considered for the evaluation of the measurements. *QI* measures the quality of the measurement for each roughness parameter, defined as a signal-to-noise ratio between the roughness-parameter-inter-position (RP-inter-position) and the roughness-parameter-intra-position (RP-intra-position). For the computed values, a ratio is determined between RP-inter-position and RP-intra-position to create histograms of *QI* values.

RP-intra-position represents the measurement variability within the iterations performed at each position (30 repetitions per surface) on the two ground surfaces. Each series has its own standard deviation, according to a given roughness parameter. RP-inter-position represents the topographical variability between repetitions (30 positions per surface) with 10 iterations (10 measurements at the same position) on the two ground surfaces. Each set of repetitions has its own roughness-parameter standard deviation.

Additionally, four new indicators based on the Quality Index Probability Density Function (*QI PDF*) have been developed to assess the reliability of the parameters under different measurement modes used and grit level measured. These indicators include the following: the mean value of *QI* (called *Mean_Q*, Equation (1)), the percentage of outliers in the raw dataset (referred to as the *%-Out* Index), the homogeneity of *QI*, which is the ability of the *QI* PDF to fit a unimodal polymorphic distribution (referred to as the *Homo_Q*), and the number of modes present in the *QI* PDF (referred to as the *NBmode* Index).

$$Mean\_Q(RP, M, G) = \frac{\sum_{i=1}^{n} QI_i(RP, M, G)}{n} \tag{1}$$

- *RP*: roughness parameter
- *M*: instrument mode
- *G*: grit level
- *n*: number of *QI* values

Homo_Q is an indicator used to assess the quality of the fitting of a chosen statistical model in relation to the *QI* PDF. First, *QI* PDF is fitted using a unimodal and polymorphic distribution, specifically the Johnson SU model [57]. The Johnson SU distribution is used here, as this is characterized by four shape parameters ($\gamma, \delta, \sigma\xi$) (Equation (2)), which offer considerable flexibility for modelling a wide range of data distributions. The shape parameter γ adjusts the curvature of the distribution, affecting its skewness and overall shape. The location parameter δ shifts the distribution along the value axis, positioning its central tendency, such as the mode or median. The scale parameter σ controls the dispersion of the distribution, influencing its spread and standard deviation. Lastly, the location parameter ξ affects the distribution symmetry and its central location, influencing its skewness and kurtosis. By convention, $\delta > 0$ and $\sigma > 0$.

$$Z = \gamma + \delta sinh^{-1}\left(\frac{X - \xi}{\sigma}\right) \tag{2}$$

Secondly, a χ^2 calculation is made between the data set and the Johnson SU fitting, to determine the 'quality' of the statistical model adjustment. The number of histogram classes for which the histograms are calculated is different. Therefore, this factor has to be taken into account for comparison purposes. Finally, thanks to this degree of freedom, we can build the *Homo_Q* indicator according to Equation (3).

$$Homo\_Q(RP, M, G) = \frac{\chi^2(RP, M, G)}{Df(RP, M, G)} \tag{3}$$

- $Df = k - 1 - p$ (Degree of Freedom)
- *k*: number of histogram classes
- *p*: number of Johnson SU model parameters

The *NBmode* represents the number of modes in the probability density function of *QI* by utilizing a procedure that counts the modes after selecting an appropriate bandwidth. A histogram is generated with an overlaid kernel density estimate, where the bandwidth is carefully chosen to ensure an accurate representation of the distribution.

In summary, the optimal configuration of indicators includes a higher value of *Mean_Q*, a lower value of *Homo_Q*, and a lower value of *NBmode* for a reliable parameter. It is noted that a low *%-Out* is preferred.

2.3.3. Roughness Parameter Ranking Method

Since a global view combining all new indicators cannot be analysed directly, a ranking strategy is adopted to identify the most reliable roughness parameters. The approach involves creating a primary criterion called severity, based on the *Mean_Q*, *Homo_Q*, and *NBmode* indicators. The percentage of outliers is excluded from the severity criterion, as data have already been cleaned (outliers are removed from data).

The severity rate is determined by the ranking position of each roughness parameter across different measurement configurations. These ranking positions are derived from the charts presented in Appendix A. A function defined and called *Rk* is used to rank the parameters from 1st to 50th (corresponding to the 50 roughness parameters calculated for the study). If two parameters have the same value for a given indicator, they share the same rank, and the subsequent parameter does not receive the next rank but skips to

the following position. The severity rate, expressed as a percentage, is calculated using Equation (4).

$$Sev = \frac{\left(Rk^{-1}(Mean\_Q) \times Rk(Homo\_Q) \times Rk(NBmode)\right)}{NP^3} \times 100 \tag{4}$$

- *Sev*: severity rate of a given roughness parameter for a specific measurement mode and grit level;
- *Rk*: ranking position of the roughness parameter (increasing order);
- Rk^{-1}: ranking position of the roughness parameter (decreasing order);
- *Mean_Q*: mean value of *QI* for a given roughness parameter in a specific measurement mode and grit level;
- *Homo_Q*: homogeneity value of *QI* for a given roughness parameter in a specific measurement mode and grit level;
- *NBmode*: number of modes of *QI* PDF for a given roughness parameter in a specific measurement mode and grit level;
- *NP*: total number of parameters (in this case, 50).

2.3.4. Summary of the Methodology

Figure 4 presents the methodology adopted to analyse the results obtained from *QI*. Firstly, the roughness parameters are plotted as timestamp visualization, parameter by parameter, for each measurement mode and grit level. At this step, three aspects are investigated: the stability through the iteration series, the topographic representativeness of the parameter regarding the measured zones, and the global way of the data populations. For the stability and the representativeness, the analysis is conducted directly through the monitoring, and hypotheses can be made about the reliability of the parameter a priori. In parallel, the *QI* values and its PDF are computed, allowing us to obtain the mean value of *QI*, the homogeneity of *QI* and the number of PDF modes.

Sometimes, roughness parameters are more prone to have outliers in their results. For this reason, it is necessary to clean the data in each case. An algorithm is used to remove these outliers, to make all the cases studied comparable. The outliers are removed from the dataset according to the MCB method as explained in Appendix C. A topographical inspection could be also performed to determine the origin of the outliers if a difference between the a priori and a posteriori result is noted, in order to try to identify the physical causes. The aim is to link the parameter behaviour with the measurement fluctuations.

A new analysis on timestamp charts can be also conduced, identical to the previous one, but without outliers, to determine firstly if the cleaning process is correct, and in order to have an idea if the parameter is reliable a posteriori through the iteration series or the topographic representativeness. In parallel, *QI* is observed again, also depending on the heterogeneity of the new *QI* values compared to a normal distribution and the number of modes in the new *QI* PDF. The goal is to determine if a good quality is obtained a posteriori by comparison of *QI* charts.

The complete set of results from the various indicators is organized according to the measuring instruments and grinding grades, to establish a ranking of the roughness parameters based on the indicator values. For each combination of instrument, grinding grade, and roughness parameter, the values of *Mean_Q*, *Homo_Q*, and *NBmode* are ranked. This ranking helps to identify the best roughness parameter in each scenario. This ranking is made according to a severity rate described in Equation (4).

After completing a ranking for each scenario, it is necessary to summarize all the rankings. A severity rate threshold is set at 5%, allowing us to count the number of times a roughness parameter falls below this limit. This will provide an overview of the most reliable and least stable parameters in our study.
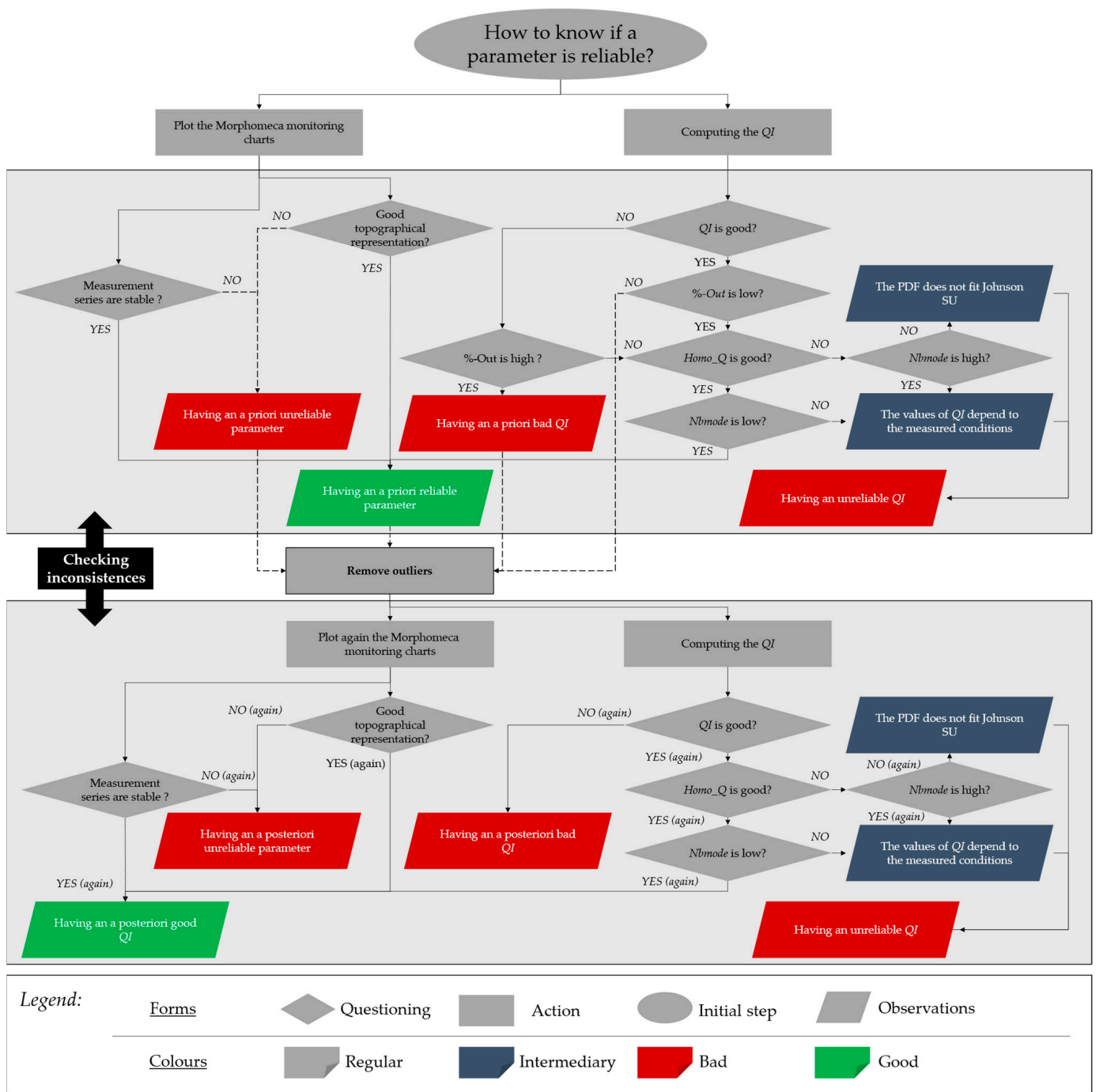
Figure 4. Flow chart representing the adopted methodology to find the reliable parameter.

3. Results and Discussion

3.1. Novel Indicators Applied on the Sa Parameter

In our previous article [54], four indexes were used to evaluate the performance of the S neox^TM (Sensofar®, Terrassa, Spain) instrument with the Sa parameter concerning the two grit levels and the different measurement modes. Figure 5 presents the results of QI and the new indicators described above. This makes it possible to know if the Sa roughness parameter is reliable.
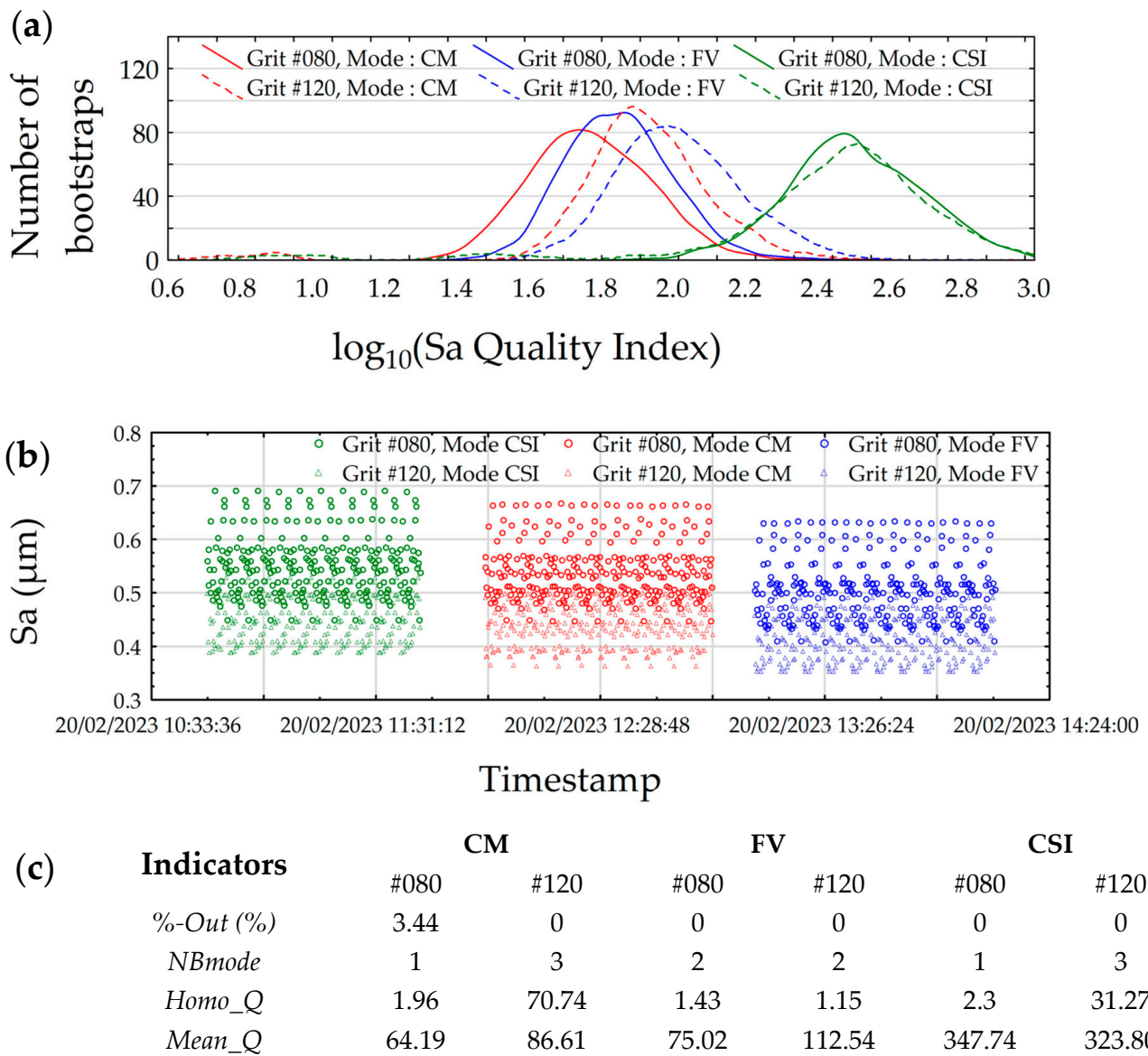
Figure 5. Quality Index computed for the Sa roughness parameter (**a**), raw Sa values versus timestamp (**b**) and calculation of the new indicators *(%-Out, NBmode, Homo_Q, Mean_Q)* (**c**) for each instrument mode and grit.

As explained in the previous article, *QI* is better for the CSI mode and *QI* is equivalent for the FV and CM modes. It can also be noted that no significant difference in *QI* is seen between two grit levels for a given instrument mode. Regarding Figure 5b, the Sa values seem to form a homogeneous population for the grit #080 (circle markers) and grit #120 (triangular markers) for each instrument mode.

This first approach allows us to compare the measurement modes and the grits, but other information is needed to choose the best roughness parameter. Sa has, globally, a low number of outliers (Figure 5c). This confirms that the populations in Figure 5b are homogeneous. The mean values of *QI* are higher for the CSI mode, as was said in a previous analysis [54], but it is also highlighted that *QI* is slightly higher for FV than CM. The PDF form plotted in Figure 5a gives information about the *QI* values distribution, i.e., the beauty of the histograms. *Homo_Q* is better for the FV mode (lowest *Homo_Q* values for the two grit levels) than the others. This means that the unimodal and polymorphic model is more capable of fitting the *QI* PDF of the FV mode. Moreover, FV has the most 'beautiful' histogram of *QI*. It can be noted that *Homo_Q* is higher for the grit #120 than the grit #080

for the CM and CSI modes. This means that the grit #080 has more 'beautiful' histograms than the grit #120, unlike the FV mode which has similar *Homo_Q* values, probably due to the smoothing effect during measurement.

The CSI and CM modes have the same number of PDF modes (one mode for #080 and three modes for #120). The one and only mode for the grit #080 confirms that the histograms are more 'beautiful' for this grit, as shown with a lower value of *Homo_Q*. The FV mode has the same number of modes for the two grits. The number of modes is therefore used to create a two-level PDF discrimination for *QI*.

By taking into account all these results, and in particular the FV results, Sa cannot be the only roughness parameter to be analysed. This is why a lot of roughness parameters from ISO and EUR [58] standards are studied in this paper, the aim being to find the most reliable parameters to describe the measurements. The number of outliers in the raw data is low for Sa, but it is not the case for the other parameters. As an example, the outlier's effect for the Sp parameter is presented in Figure 6.
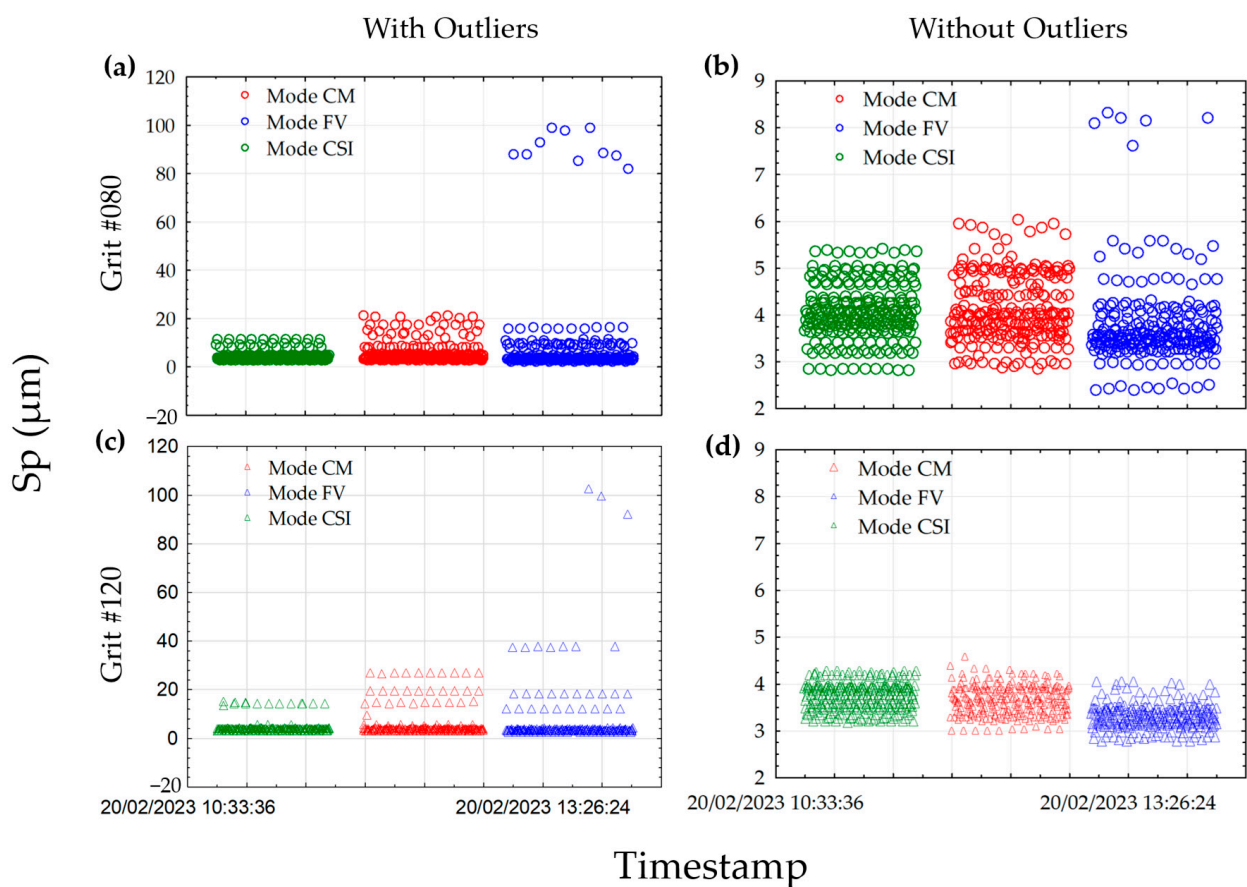

Figure 6. Raw values of the Sp roughness parameter versus acquisition time, as presented in Morphomeca Monitoring: with outliers for grit #080 (**a**) and grit #120 (**c**), without outliers for grit #80 (**b**) and grit #120 (**d**).

The Sp parameter is presented here, as this parameter is very sensitive to map fluctuations, and data clean-up could be needed. The average percentage of outliers for the grit #080 is 16.89% (+2.78%/−4.89%) and 11.55% (+4.48%/−6.55%) for the grit #120. It can be noted in Figure 6 that the range of the Sp values has the same order of magnitude for the grit #080 and #120, both before and after removing outliers. The difference in the data population between the two grits is therefore more easily established, and the Sp values for the grit #080 are more dispersed than the grit #120, due to a higher relief in topography. It can therefore be questioned how the removal of these outliers influences the *QI* PDF.

3.2. Example of Cases of QI Regarding the Homogeneity of PDF, the Number of PDF Modes, and the Percentage of Outliers with and Without Outliers

As introduced earlier, three indicators are built based on the *QI*. These characterize the *QI* to determine the reliability of roughness parameters regarding their measurement representativeness and repeatability.

Figure 7 presents various cases of indicator performance with no removed data (with outliers), including the best *Mean_Q* and the worst *Homo_Q* (Figure 7a), the worst *Mean_Q* (Figure 7b), the highest *NBmode* (Figure 7c), the best *Homo_Q* (Figure 7d) and the lowest (Figure 7e) and highest (Figure 7f) *%-Out*. Table 2 presents the values of the indicators associated with Figure 7.
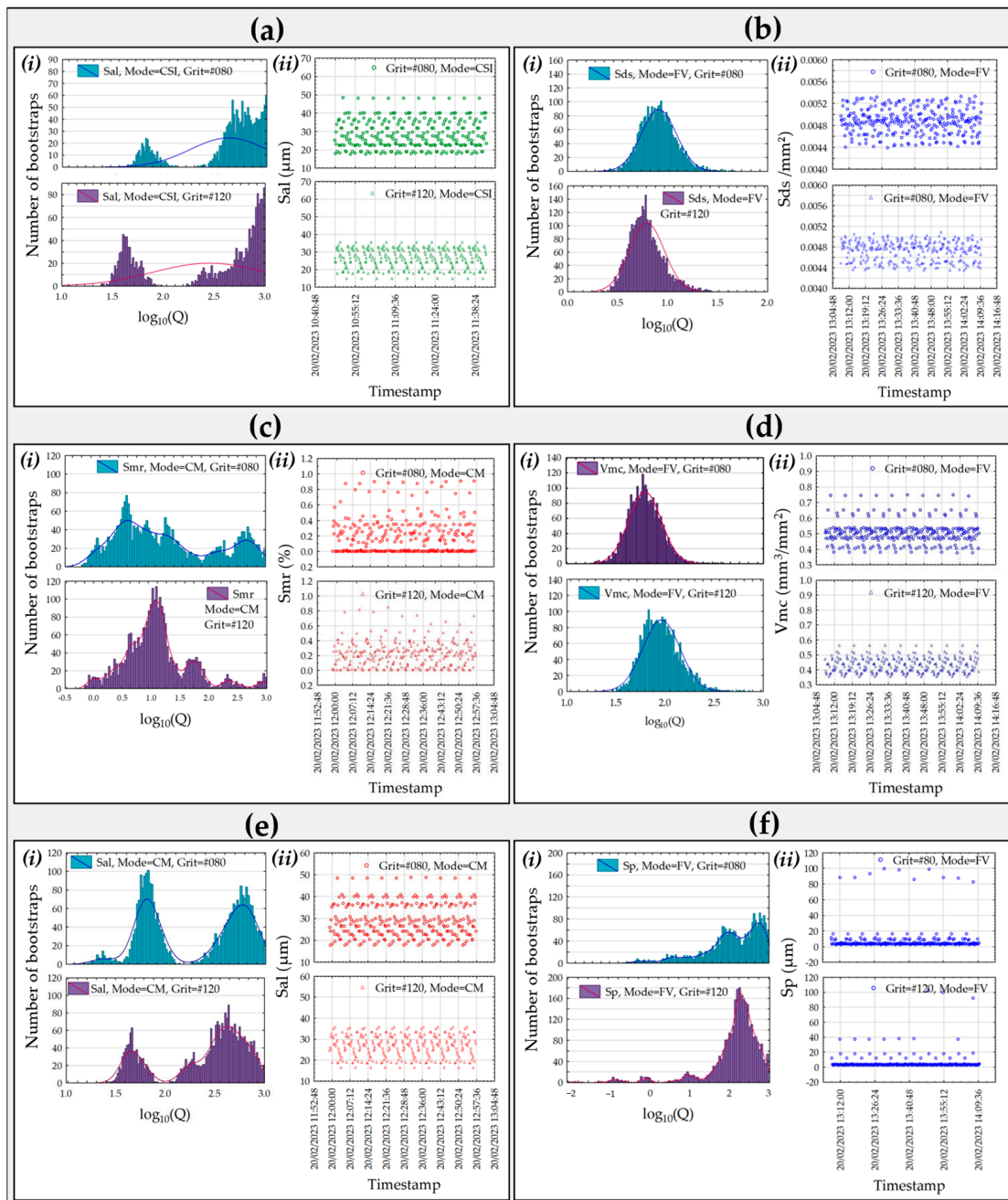

Figure 7. *QI* PDF (**i**) and timestamp graph (**ii**) with outliers for different cases of indicator performance: the best *Mean_Q* and worst *Homo_Q* (**a**), the worst *Mean_Q* (**b**), the highest *NBmode* (**c**), the best *Homo_Q* (**d**), the lowest *%-Out* (**e**) and the highest *%-Out* (**f**).

Table 2. Values of the indicators for each performance case with outliers illustrated in Figure 7.

Observation		Instrument Mode	Roughness Parameter	Grit	
Indicator	**Case**			**#080**	**#120**
Mean_Q	Best	CSI	Sal	532.99	480.48
Homo_Q	Worst			150.13	250.72
Mean_Q	Worst	FV	Sds	8.80	6.71
NBmode	Highest	CM	Smr	2	4
Homo_Q	Best	FV	Vmc	1.43	0.91
%-Out (%)	Lowest	CM	Sal	0	0
%-Out (%)	Highest	FV	Sp	21.37	14.33

In general, no major difference in *Mean_Q* is observed between the two grits for each case, indicating that the parameters are consistent across grit levels. It is important to note that the parameter is selected based on a global ranking across all instrument modes. It appears that some *QI* PDF are clearly not smooth and contain multiple modes, more especially in Figure 7a,c,e,f. The irregular shapes are highlighted by the number of modes, the homogeneity, and the percentage of outliers. In the study, the Sal parameter is highlighted three times as a specific parameter: it is ranked as one of the best *Mean_Q* values for the CSI mode in Figure 7a, and one of the lowest *%-Out* values for the CM mode (Figure 7e), but Sal is also highlighted as the worst parameter for *Homo_Q* for the CSI mode. The Sds parameter for the FV mode has one of the worst *Mean_Q* values but a low number of PDF modes. Additionally, the Smr parameter shows a high number of PDF modes for the grit #120 and for the CM mode, while the Sp parameter has one of the highest numbers of outliers.

Given the percentage of outlier points for certain roughness parameters, it may be necessary to clean the data before calculating the Quality Index and the new indicators. However, this cleaning is not intended to make the 'poor parameters' reliable, but rather to prevent values that deviate too much from the parameter data from being taken into account (graphs presenting parameter values versus time). This allows us to obtain valuable indicators for roughness parameters having a few unstable points, which disturb the *QI* results.

Similar to Figure 7, Figure 8 presents the same cases of indicator performance after outlier removal, allowing for a comparison of the indicator values with (Table 2) and without outliers (Table 3). Overall, it is evident that the amplitudes of *QI* PDF remain consistent for the charts with removed outliers, except in the case of a higher percentage of outliers. This indicates that the outlier removal method does not significantly affect the *Mean_Q*, *Homo_Q*, or the number of mode indicators. It is also reassuring that the shapes of the *QI* distributions are generally similar. The outlier percentage is remembered, and is the same as before (Table 2).

Table 3. Values of the indicators for each performance case without outliers illustrated in Figure 8.

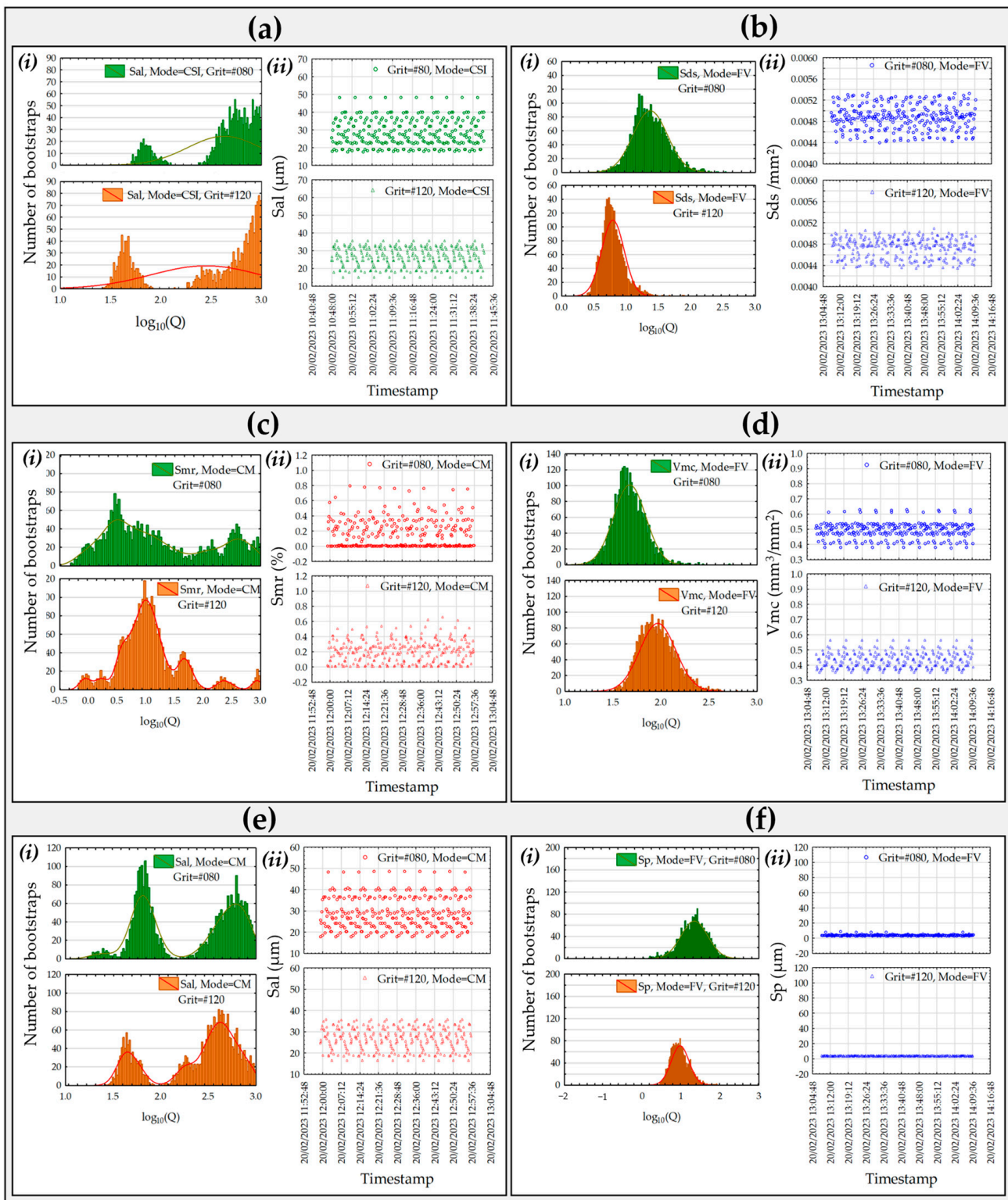| Observation		Instrument Mode	Parameter	Grit	
Indicator	**Case**			**#080**	**#120**
Mean_Q	Best	CSI	Sal	531.26	472.80
Homo_Q	Worst			96.29	311.17
Mean_Q	Worst	FV	Sds	8.87	6.73
NBmode	Highest	CM	Smr	2	5
Homo_Q	Best	FV	Vmc	2.51	1.94
%-Out (%)	Lowest	CM	Sal	0	0
%-Out (%)	Highest	FV	Sp	0	0

Figure 8. *QI* PDF (**i**) and timestamp graph (**ii**) without outliers for the same cases of indicator performance presented in Figure 7: initially the best *Mean_Q* and worst *Homo_Q* (**a**), initially the worst *Mean_Q* (**b**), initially the highest *NBmode* (**c**), initially the best *Homo_Q* (**d**), initially the lowest *%-Out* (**e**) and initially the highest *%-Out* (**f**).

For example, a notable difference in *QI* PDF is observed in the case of the Sp parameter, due to the significant number of removed data: a high percentage of outliers is computed (21% for grit #080 and 14% for grit #120). Appendix D shows the indicators without outliers

for Sp and the FV mode (Figures A3 and A4). Thus, the outlier removal method only impacts *QI* PDF for parameters with a higher percentage of outliers, validating the method application. It is also worth noting that the *Mean_Q* values are sometimes slightly higher in the cleaned *QI* results, because the data cleaning algorithm reduces the topographical representation (roughness parameter inter-standard deviation) without modifying the measurement fluctuation (roughness parameter intra-standard deviation). This results in an increase in *QI* (signal-to-noise ratio).

3.3. Ranking of Roughness Parameters

To conclude, while these indicators effectively describe the behaviour of roughness parameters, a case-by-case analysis for all parameters is impractical. This raises the important question of how a multi-parameter analysis can be conducted based on these indexes, emphasizing the need for a more integrated approach.

Figure 9 gives an example of the ranking detailed in Appendix E, showing the severity values in percentage for the three instrument modes and the two grit levels. It appears that the severity rates are generally higher for the grit #080 for the CM and CSI modes, likely due to the greater texture. This indicates that the roughness parameters have generally a low quality and a poor PDF for the grit #080 compared to that for the grit #120. However, this is not the case for the FV mode, where higher values are observed for the grit #120. As previously shown, the FV mode behaves differently from the other two modes when comparing grits.
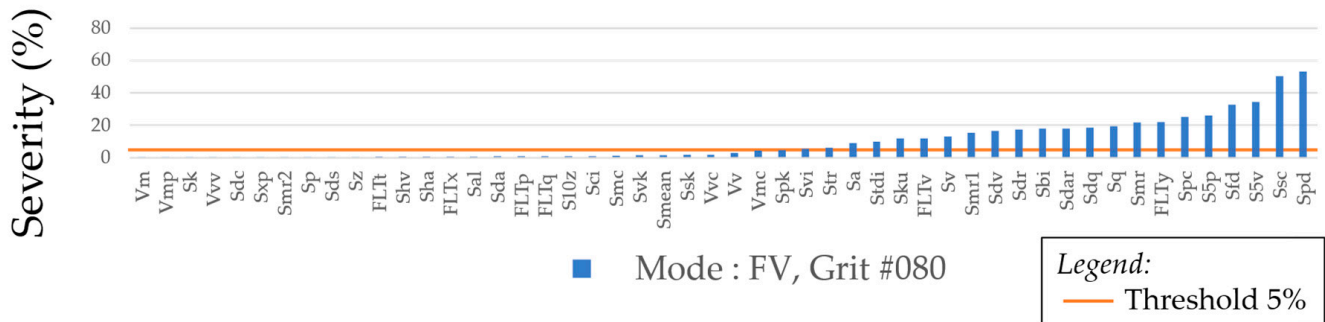

Figure 9. Example of roughness parameter ranking, depending on the severity rate.

A threshold of 5% is chosen to distinguish the reliable roughness parameter and unstable parameters. A 5% threshold value is used as a convention, representing the level at which the severity rate of a roughness parameter is considered unstable based on the indicators *Homo_Q*, *Mean_Q*, and *NBmode*. These indicators are calculated from the Quality Index (*QI*) probability density function, to determine whether the *QI* values can be considered for further analysis. In each case, approximately half of the roughness parameters are below 5% showing the threshold is correctly chosen, but only some parameters are common for all grits and instrument modes.

Figure 10 illustrates how often a parameter falls below the 5% severity rate, as shown in Appendix E. The six scenarios are analysed based on the measurement conditions. The occurrence values range from 0 to 6, with 0 indicating the worst parameters (those that consistently exceed 5% severity) and 6 indicating the best parameters (those that consistently stay below 5% severity). For example, Sa is higher than 5% of severity for the cases FV mode/grit level #080, CM/#120 and CSI/#120. The occurrence value is thus 3. In addition, it can be noted that each occurrence is represented in Figure 10, showing the 5% threshold is correctly chosen.
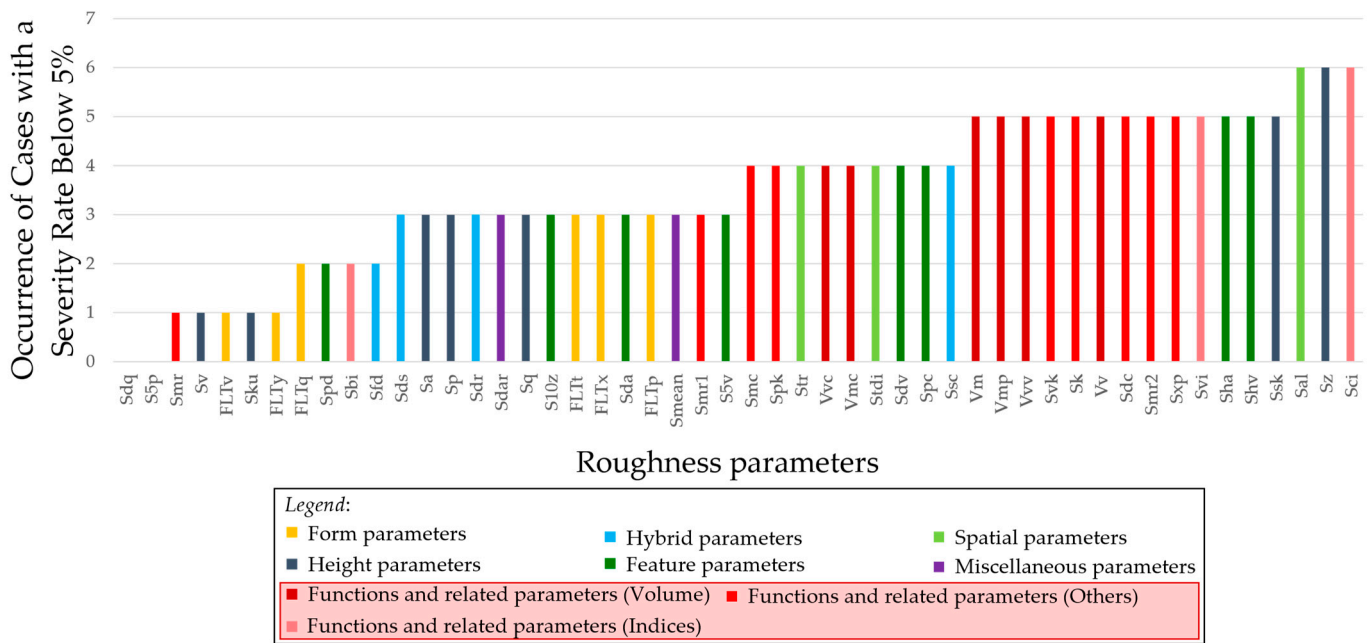
Figure 10. Occurrence of the parameters having a severity rate below 5% for each grit level and instrument mode presented in Appendix E.

Notably, the best roughness parameters are Sal (spatial parameter), Sz (height parameter), and Sci (functional indice) with an occurrence of six (six times below 5%). Additionally, Vm, Vmp, Vvv, Svk, Sk, Vv, Sdc, Smr2, Sxp, Svi, Sha, Shv, and Ssk can also be considered reliable parameters, as they appear in five out of six cases. It appears that the least reliable roughness parameters are clearly Sdq and S5p, because in all cases they always have more than 5% of severity rate. It could be considered that the Smr, Sv, FLTv, Sku, FLTy parameters are unstable too.

More precisely, the focus is on the best and the worst ranked parameters, to make the link between the parameter definition and the obtained results (physical causes):

- The Sal parameter (Texture Aspect Ratio of the Surface) represents the autocorrelation length of the map, expressed in wavelength. A higher Sal value indicates a greater presence of long wavelengths within the map. The Sal parameter is a key metric used to evaluate the anisotropy of a surface, meaning the directional properties of the patterns or textures present. It is especially useful for surfaces with regular, oriented textures, such as those produced by grinding or lapping processes, which often result in surfaces with distinct striations. For striated surfaces, such as those produced by grinding or polishing, Sal is directly related to the width and spacing of the striations. A surface with wide, well-aligned striations will have a low Sal, indicating strong directionality. Conversely, if the striations are irregular or vary significantly in spacing, Sal may increase, reflecting a loss of clear directional alignment. A high *Mean_Q* value for Sal indicates low dispersion of the Sal values across the iteration series, highlighting broad topographic characterization. For the manufactured surfaces (#080 and #120), this suggests that the long wavelengths (wide cutting scratches on the surface) are dependent on the different measured areas, as evidenced by the wide variation in the Sal values. This shows that Sal is a good parameter for distinguishing between different measured areas, particularly regarding the noise observed in the iteration series. However, it is important to note that while variations in wavelength are averaged when calculating Sal, small variations within an iteration series may have minimal impact on the Sal values. Additionally, *Homo_Q* of Sal is not particularly strong, indicating that the *QI* ratio, which includes both intra-position and inter-position standard deviations of Sal, may not be stable across different measured

areas or throughout the iteration series (i.e., zone-dependent or time-dependent). One of the main limitations of Sal in this context is its sensitivity to the size of the striations. If certain striations are significantly larger or more irregular than the rest, they can disproportionately influence the Sal value, even if they are few in number. This creates a high statistical variability, making it difficult to obtain a representative measure of the surface's anisotropy. To address this variability, a highly effective approach is to increase the measurement area using a technique called stitching. This involves combining multiple local measurements of a surface into a single, larger image. Stitching allows for the measurement of a greater portion of the surface, thus incorporating more striations into the analysis. By increasing the number of measured striations, the influence of rare, large, or irregular striations is minimized, leading to more reliable and representative Sal measurements.

- The Sz parameter represents the maximum height of the surface, defined as the difference between the highest peak and the deepest valley. The Sz ranking is reliable, characterized by low *Homo_Q* and *NBmode* values, which suggest a well-defined histogram and a satisfactory *Mean_Q* value. Due to differences in topographic features between measured areas, a high dispersion in Sz can be observed. When taking multiple measurements at different locations on a randomly textured surface, such as a ground surface, the Sz parameter can exhibit significant variability, which is closely related to the extreme value theory. Since Sz is based on the highest peaks and lowest valleys of the surface, its value is highly sensitive to local irregularities, such as isolated large peaks or deep pits. On a surface with random striations and irregular features, different measurement locations may capture different extreme values, leading to a wide range of Sz results. This variability arises because each measurement could include a rare or extreme feature that disproportionately impacts the Sz value, despite the overall surface texture being relatively homogeneous. According to extreme value theory, which models the behaviour of maxima or minima in random systems, such extreme events are expected to occur infrequently, but can significantly influence the outcome when they do. This results in Sz being a less reliable indicator of the overall surface roughness, as it is heavily influenced by outliers rather than reflecting the typical texture of the surface. To address this variability, larger measurement areas using stitching techniques can be employed to capture a more representative sample of the surface, averaging out extreme features. Extreme value theory can also be applied to better understand and model the behaviour of these extreme surface features, particularly when they are critical to the application [59]. However, the ratio between topographic representativeness and noise in the iteration series is sufficient to consider Sz as a qualitative parameter, particularly given the robustness of the *QI* for every measured area and iteration series, as reflected in the well-formed histogram.

- The Sci parameter is a roughness index that indicates core fluid retention, calculated as the ratio of void volume in the core zone (from 5% to 80%) to the RMS deviation (Sq). *Mean_Q* of Sci is generally good, outperforming Sz, due to high deviations between different measured areas, which is linked to variations in the surface topographies. *NBmode* of Sci, while higher than Sz and Sal, is still acceptable. This could be attributed to the presence of high peaks on the surface (groove pile-up) or third core inclusions, as the calculation of Sci is highly sensitive due to its 5% threshold, leading to multiple modes in *QI* PDF. Nevertheless, *Homo_Q* remains favourable for this parameter, indicating that the *NBmode* values are closely aligned or nearly merged.

- The Sdq parameter represents the RMS slope of the surfaces, and appears to be unreliable in terms of ranking. However, it is noteworthy because it indicates that slope is a highly sensitive feature of the surface [49]. Despite this, Sdq performs well in terms of *QI*, showing that the ratio of deviation between topographical representativeness and noise in the iteration series is generally good. However, the high *NBmode* and *Homo_Q* values suggest a local instability in Sdq *QI* values, both intra- and inter-position. This instability likely stems from the physical limitations of the instruments in measuring

slope. When the slope limit is reached, some pixels may be measured inconsistently, leading to variable pixel quality [60]. The Sdq parameter is crucial for assessing surface roughness, but it is highly sensitive to the sampling interval used in measurements. This sensitivity arises because the Sdq calculation involves the derivative of the surface profile, and any noise present in the data can significantly affect the accuracy of this derivative. A larger sampling interval can amplify noise during derivative calculations, as it may exaggerate random fluctuations in the data, leading to less accurate Sdq values. Conversely, a smaller sampling interval can enhance precision by capturing more detailed surface features, but it increases the data volume and may also magnify the effects of measurement noise. To mitigate these issues, several approaches can be employed. Data filtering techniques, such as the Gaussian filter [61], can smooth the data before derivative calculation, reducing noise while preserving essential surface characteristics. Choosing an optimal sampling interval is essential to balance detail and noise effects. Advanced interpolation methods, like B-spline interpolation, can offer more robust performance against noise compared to Lagrange interpolation by providing a smoother approximation of the surface profile. Our sensitivity analysis can help us to understand how variations in the sampling interval impact Sdq calculations, allowing for adjustments in measurement and processing methods, to ensure reliability. By addressing our indexes and implementing appropriate solutions, the accuracy and reliability of Sdq measurements can be significantly improved.

- The S5p parameter belongs to the segmentation-based family. The Wolf pruning algorithm is used to eliminate insignificant motifs by merging smaller ones into larger ones. This parameter is sensitive to the calculation method, representing the average height of the five peaks with the highest global peak height within the defined area. As a result, the area computation is sensitive to small variations in surface iteration series, as evidenced by a poor ranking of *Mean_Q* for this parameter. Furthermore, the high *NBmode* and *Homo_Q* values indicate instability in the inter- and intra-position standard deviations of S5p values. The variability in segmentation caused by noise means that the significant peaks identified may differ from one measurement to another, complicating the consistency and accuracy of the results. To mitigate this issue, several approaches can be employed. Data filtering techniques, such as filters [62], can smooth out the noise before segmentation, helping to preserve essential surface characteristics while reducing random fluctuations. Performing repeated measurements at the same location and obtained a mean map can also help to lessen the impact of noise and provide a more stable assessment of surface quality [50]. Advanced pruning methods, like the Wolf pruning threshold, can be used to refine the results by focusing on the most significant data points and minimizing the influence of noise. By addressing the challenges of noise and segmentation variability through these strategies, it is possible to achieve more reliable and accurate evaluations of surface quality.

An analysis of the roughness parameter family reveals that the functions and related parameters (highlighted by a red box) are generally reliable, particularly the volume parameters. However, it also indicates that the form parameters are globally unstable (in yellow). As for the height parameters, they exhibit either reliability or instability, likely due to the calculation method which directly depends on the heights of the maps, and can cause some instabilities in results. No further comments can be made on the other roughness parameter families, as the parameters within them are uniformly represented in the ranking. Finally, the severity rate can describe as a Quality indicator of a Quality index, allowing us to validate whether a Quality index computed on roughness parameter values is good or not. This answers the following question: if a set of parameters is known for its physical relevance, which is the most reliable parameter?

4. Conclusions

Previously, four indexes were developed to characterize the measurements performed with a Sensofar S neox™ (Sensofar®, Terrassa, Spain): quality index, stability index, drift

index and relevance index. Each index was calculated on the Sa values computed from topographies obtained according to a specific measurement plan, named Morphomeca Monitoring. In this paper, only the quality aspect is studied through the Quality Index (*QI*) and four new indicators are created based on this index: the mean *QI* value (*Mean_Q*), the *QI* homogeneity (*Homo_Q*), the number of modes in the *QI* probability density function (*NBmode*) and the percentage of outliers of the parameter values (*%-Out*). These indicators were firstly studied for the Sa parameter, then for 50 roughness parameters (ISO and EUR standards).

If only the Sa parameter is considered, the analysis of *QI* across different instrument modes and grit levels shows that the CSI mode consistently has the highest *Mean_Q*, while the FV and CM modes perform similarly. The FV mode is notable for its superior histogram homogeneity (*Homo_Q*) and more consistent *QI* distributions, which are less influenced by grit levels. However, the FV mode tends to smooth the surface topography, which can introduce bias in the conclusions. For example, no significant differences are observed between grit #080 and grit #120 across any instrument modes. This limitation highlights the need for a multi-parameter approach to fully capture surface characteristics.

Additionally, the data of the Sa parameter have relatively few outlier values, which is why an outlier removal method was applied in this study. This method is necessary to harmonize parameters with one another. Generally, removing outliers does not significantly affect key indicators like *Mean_Q* or *Homo_Q*, except in cases with a high percentage of outliers, such as the Sp parameter.

To evaluate the roughness parameters across different instrument modes and grit levels, a ranking system was established using severity rates. A 5% threshold was set to identify reliable parameters. Through this process, Sal, Sz, and Sci emerged as the most reliable parameters, while others like Sdq and S5p were consistently unstable. The analysis also showed that function-related parameters, especially those related to volume, tended to be more reliable, whereas form parameters were generally unstable.

The proposed method adopts an overview of a large set of roughness parameters, allowing us to investigate a complementary point of view regarding the surface properties and features. The method takes into account the fact that the measurements could be performed with different instruments and different levels of surface generation intensity. However, it can be noted that just because a parameter is reliable, it does not necessarily have physical significance in the study of the surface generation process.

All of the approach is based on the *QI* but, as shown in [54], others indexes such as the Drift Index (DI), Stability Index (SI) and Relevance Index (RI) exist, and could be included in the study. A future work including all indexes is scheduled to find the criteria to rank roughness parameters by following a global method allowing us to determine the best instrument mode to measure a specified manufactured surface.

In the bibliography, a lack of knowledge is identified regarding the reliability of the roughness parameters with regard to a specific measurement condition (instruments and measurement plan) and intrinsic properties of a surface. These findings underscore the complexity of selecting appropriate roughness parameters and the importance of using a comprehensive, integrated approach to achieve accurate and reliable surface measurements.

To conclude, this study proposes a novel method based on the statistical analysis of roughness parameters and a severity ranking system to highlight the most reliable parameters computed from surface topographies obtained using a set of instruments and a specific measurement strategy. This method can be applied to all surface types and for other roughness parameters, even if only one instrument is analysed, although the ranking step will show only two values (1 for parameters below 5% and 0 for parameters above 5%). When only a single instrument is studied, the results become more specific, and are not meant for comparative analysis.

As a future perspective, a complementary study could be conducted on other surface conditions, such as sandblasting, femto-laser, or oxidation, to identify the most reliable parameters, regardless of surface type. This would help determine if certain parameters

are sensitive enough to be attributed to specific surface types. In such cases, a particular parameter could be linked to a specific device/surface combination to monitor measurement quality. It can also be noted that the influence of instruments settings is not taken into account in the field of this study. Another work can be conducted to show the influence of magnification, acquisition velocity or other relevant settings on the roughness parameter reliability, the quality index or the others indexes developed in [54].

Author Contributions: Conceptualization, M.B.; methodology, M.B. and C.M.; software, F.B. and M.B.; validation, J.L., D.P.M. and F.B.; formal analysis, M.B. and C.M.; investigation, M.B.; resources, D.P.M.; writing—original draft preparation, C.M.; writing—review and editing, C.M., M.B. and J.L.; visualization, J.L.; supervision, M.B. and F.B. All authors have read and agreed to the published version of the manuscript.

Conflicts of Interest: Authors David Páez Margarit and François Blateyron were employed by the company Sensofar Metrology and Digital Surf. The remaining authors declare that the research was conducted in the absence of any commercial or financial relationships that could be construed as a potential conflicts of interest.

Appendix A. Optical and Geometrical Surface Properties, with Regard to Instrument Performance

Table A1. Instrument performance, with regard to intrinsic surface properties.

Type	Properties	Definition	Instrument Performance		
			CSI (VSI) Rating	CM (Field) Rating	FV Rating
Optical	Reflection (mirror, polished surfaces)	Light reflected by the surface	+++ [63–67]	++ [68]	+
	Absorption (carbon layers, copper oxides, black ceramics, textured silicon)	Ability to absorb certain wavelengths	+	+	+
	Transmission (optical lens, transparent layer)	Ability of light to pass through the surface	+++ [21,22,60,69]	++ [70,71]	+ [70]
Geometrical	Flatness	Degree from which a surface deviates from a perfectly flat plane	+++ [22,72]	+	+
	Form	Degree from which a surface bends or curves	++ [21,73,74]	++ [20]	+++ [75]
	Local slopes	Local gradient of surfaces	++ [60,71,73,76,77]	+++ [78–80]	+ [81]
	Texture (skin, grounding, turning, textile)	Including roughness, waviness, and pattern directionality	++ [16,81–84]	++ [81,85,86]	+++ [18,81,85,87]

Table A1 presents a comparative analysis of the CSI, CM, and FV instruments in relation to surface properties, indicating the affinities of each instrument using a notation system (+, ++, +++) in increasing order.

The optical and geometrical properties are detailed here:

- Optical properties:

  o Reflection: the light is either reflected in a single direction, like a mirror, or diffusely reflected in many directions, as seen on matte surfaces. The FV instruments are more sensitive to reflection than the CSI and CM instruments, due to the focusing criteria (maximum contrast gradient between a pixel and its neighbours). It is explained in [65] that the mirror measurement by conventional FV is not possible.

  o Absorption: this is the ability of a surface to absorb certain or all light wavelengths, converting light energy into heat or other forms of energy. In other words, this type of surface could be assimilated as a light trap. CSI is very sensitive to absorption because the interferogram is based on the succession of fringes and their intensities, while FV takes into account the contrast gradient between one pixel and its neighbours, and CM cannot measure without light projection on the CCD sensor through the pin hole. In this case, Atomic Force Microscopy (AFM) is commonly chosen, as in [88,89], but the measurement size and Z-amplitude are limited.

  o Transmission: this refers to the capability of the light to pass through a surface. Transmission is high for transparent materials and almost zero for opaque materials. CSI is not too sensitive if a good scanning range is set [21], because it uses constructive or destructive waviness [22]. As CM uses the principle of laser focalization, it can be disturbed due to the upper and lower interface, as explained in [70]. The FV, based on contrast criteria, cannot be used, due to the lack of contrast gradient on the surface, as explained in [70]. CSI could be slightly better than CM because noise could appear for CM, but CM is able to detect a change in the refractive index.

- Geometrical properties:

  o Flatness: this is the degree to which the concerned surface deviates from a perfect plane. The majority of work with measurements on flat surfaces is performed with CSI or AFM instruments. CSI instruments, particularly Phase Shifting Interferometry (PSI) instruments, are preferred for flat surfaces, though Vertical Scanning Interferometry (VSI) can also measure flatness, but not with the same precision.

  o Form: this refers to the global shape of the specimen. Measuring form requires a high Z-scanning range, and in most cases, instruments using Focus Variation are predisposed to measure this type of surface. CSI instruments, especially VSI, are also capable of measuring form, but not on as large a scale as FV [21], and the scale for CSI is more relative to low-frequency waviness in this case. The Numerical Aperture (NA) is an important criterion for form measurement with CSI. CM instruments have comparable performance to CSI for form measurement, but like CSI, CM instruments have errors that increase with the specimen slope [20,74].

  o Local slope: this refers to the local variation in relief in surface morphology, calculated from heights on measured topographic maps between two pixels, commonly called the surface gradient. According to the literature, the most effective instrument for measuring the local slope is the CM instrument, due to its small lateral resolution. CSI instruments can also be effective, but the numerical aperture of the lenses may limit acquisition and cause measurement errors, due to a lack of signal. FV instruments are generally not capable of measuring the local slope because of the smoothing effect inherent in this technology [81].

  o Texture: this refers to the entirety of surface features, representing the global definition of surface characteristics. Surface texture can be seen as a summary of the geometrical properties of the surface. The ISO 25178-2 [58] defines a set of scale-limited features in three class: areal (hill and dale), line (courses line and ridge line) and point (peak, pit and saddle point). This classification is usually used in surface segmentation analysis. Generally, all instruments with sufficient magnification or stitching area can measure surface texture, but with their own abilities. FV instruments are more suited for this task, due to their capability of handling high roughness levels (when surface texture is high), and because a global surface description is often required. CM and CSI instruments can be limited in this application at equivalent magnification

because a large field of view (FOV) is required for texture measurement, but they can also provide complementary information when small-scale textures need to be measured. Some textures, such as skin surfaces, can pose challenges due to light traps, especially with CSI instruments. Textures that include step-like features can also be problematic for CM and CSI instruments as they may lead to overestimation around the measured features.

Appendix B. Features of the Raw Surfaces

The ground surface (#080) measured in this paper is presented in Figure A1. Understanding the tribological aspects is essential for processing the surface topographies and comprehending the behaviour of roughness parameters. It is shown that the ground surfaces are composed of multi-scale features created by the abrasive grains, as in [90]. These features include deeper valleys at higher scales, resulting from the cutting mechanism of the abrasive particles, as described in [11,91]. At a scale larger than the grain-size distribution, the edges of the grains tend to be smoother, leading to less-pronounced indentations and less-important valleys. Peaks become more prominent, and debris, including large metal flakes mixed with abrasive particles, can be embedded in the surface. This mix of adhesive and abrasive wear, as detailed in [92], further influences the surface roughness characteristics.
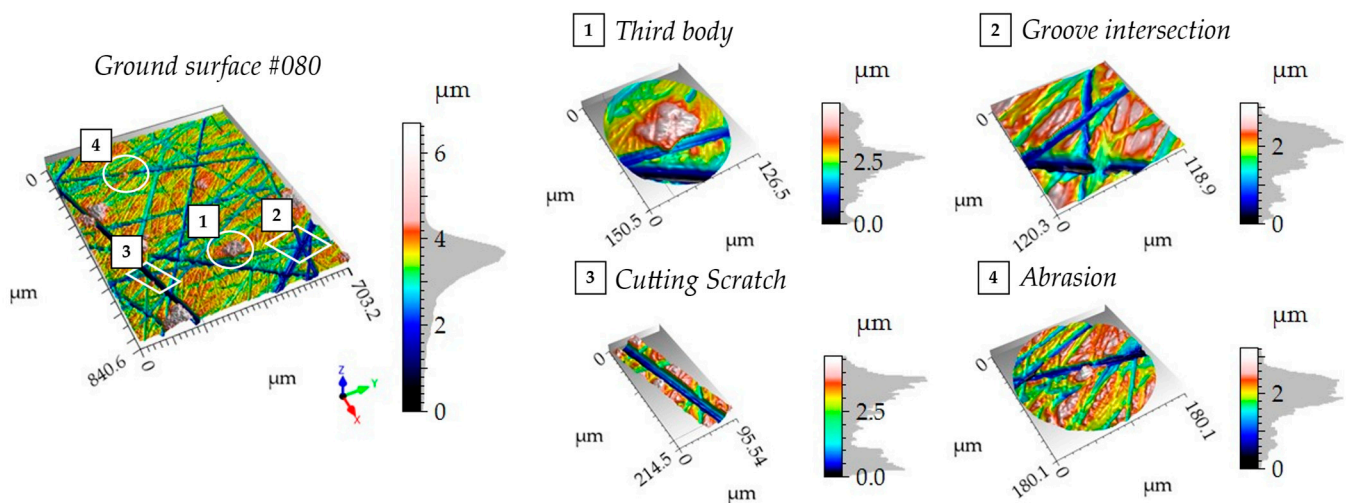

Figure A1. Surface features obtained by grinding process on TA6V.

Appendix C. The Outlier Detection Method

The outliers are detected with an algorithm presented in [93]. Among the four methods presented in this paper, the Boxplot Method (BPM) is used here (Figure A2). This method is based on the first quartile $Q1$ (25th percentile) and the third quartile $Q3$ (75th percentile). Two thresholds are defined from these statistics: a lower cutoff (LC) and an upper cutoff (UC) (Equations (A1) and (A2)).

$$LC = Q1 - 1.5 \times IQR \tag{A1}$$

$$UC = Q3 + 1.5 \times IQR \tag{A2}$$

- $IQR = Q3 - Q1$: Interquartile Range

This outlier's detection method is robust because it is based on the $Q1$ and the $Q3$ and is less sensitive to outliers. In addition, the distribution skewness does not impact the outlier's detection, because the median is not taken into account (just the $Q1$ and the $Q3$).

Figure A2. Focus variation (FV), grit #080.

Appendix D. Overview of Indicator Comparison with and Without Outliers for the Given Instrument Modes and Grits
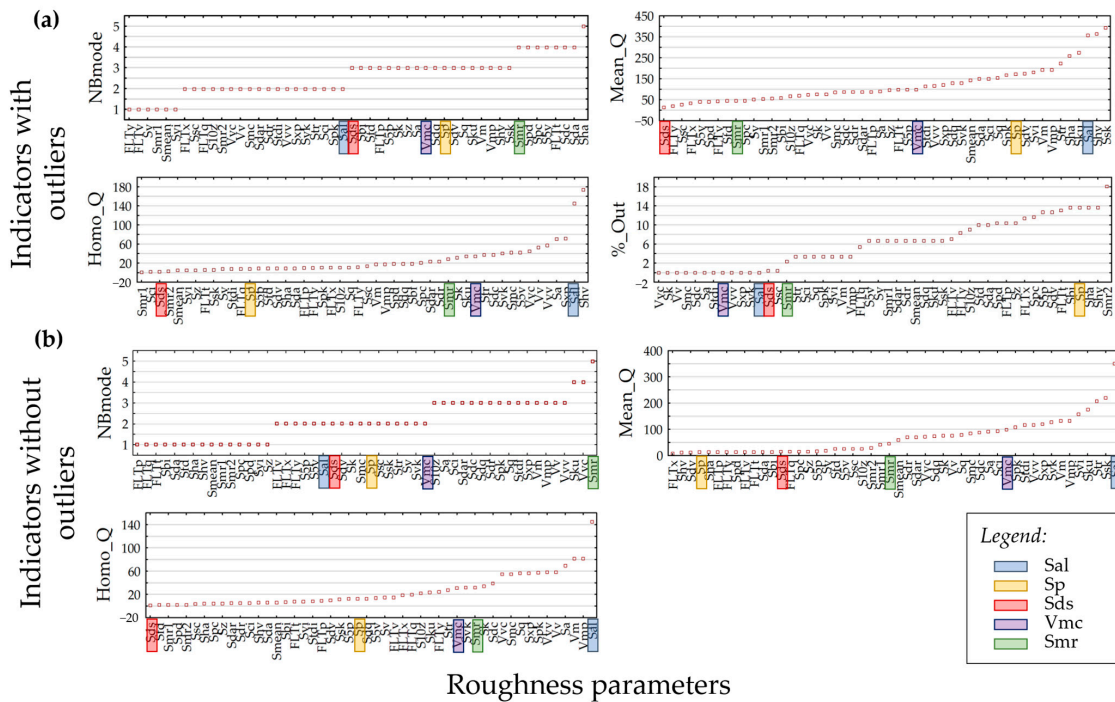
Appendix D.1. Focus Variation (FV), Grit #080

Figure A3. Ranking of the roughness parameters for the indicators (*NBmode, Mean_Q, Homo_Q*), for the FV mode and the grit #080: with outliers (**a**) and without outliers (**b**).

Appendix D.2. Focus Variation (FV), Grit #120

Figure A4. Ranking of the roughness parameters for the indicators (*NBmode, Mean_Q, Homo_Q*), for the FV mode and the grit #120: with outliers (**a**) and without outliers (**b**).

The *Homo_Q* values of the parameters Spc, Sdq and Ssk (respectively, 500, 2500 and 3000) are not displayed in Figure A4a because the other values are not clearly visible, due to their higher magnitude.

Appendix D.3. Confocal Microscope (CM), Grit #080

Figure A5. Ranking of the roughness parameters for the indicators (*NBmode, Mean_Q, Homo_Q*), for the CM mode and the grit #080: with outliers (**a**) and without outliers (**b**).

Appendix D.4. Confocal Microscope (CM), Grit #120

Figure A6. Ranking of the roughness parameters for the indicators (*NBmode*, *Mean_Q*, *Homo_Q*), for the CM mode and the grit #120: with outliers (**a**) and without outliers (**b**).

The *Homo_Q* value of the parameter Sp (1800) is not displayed in Figure A6a because the other values are not clearly visible, due to their higher magnitude.

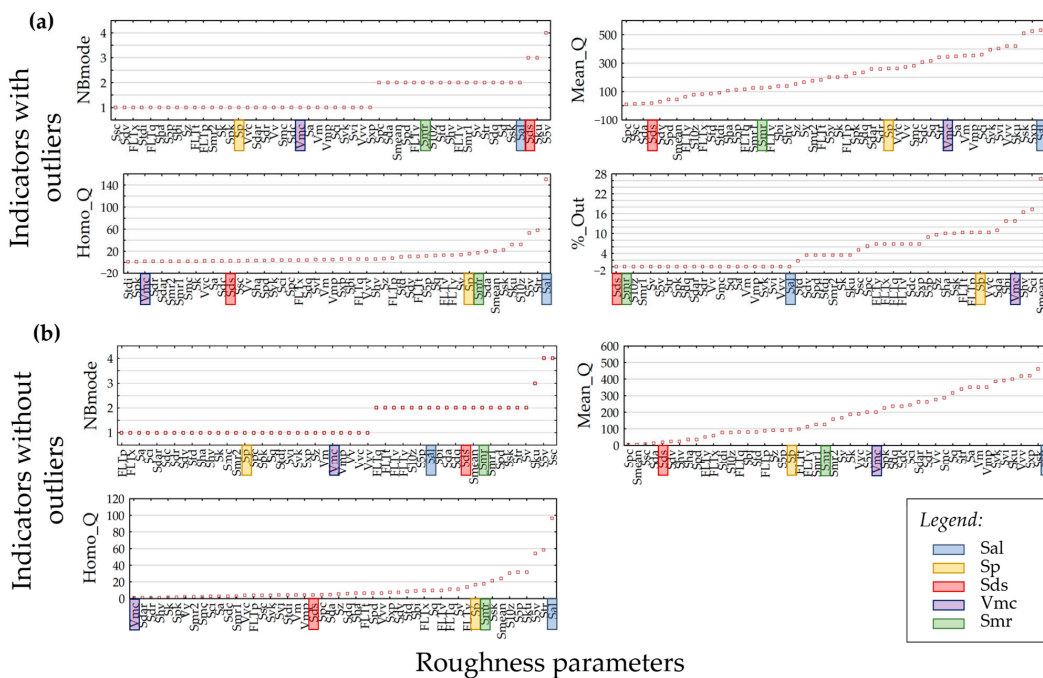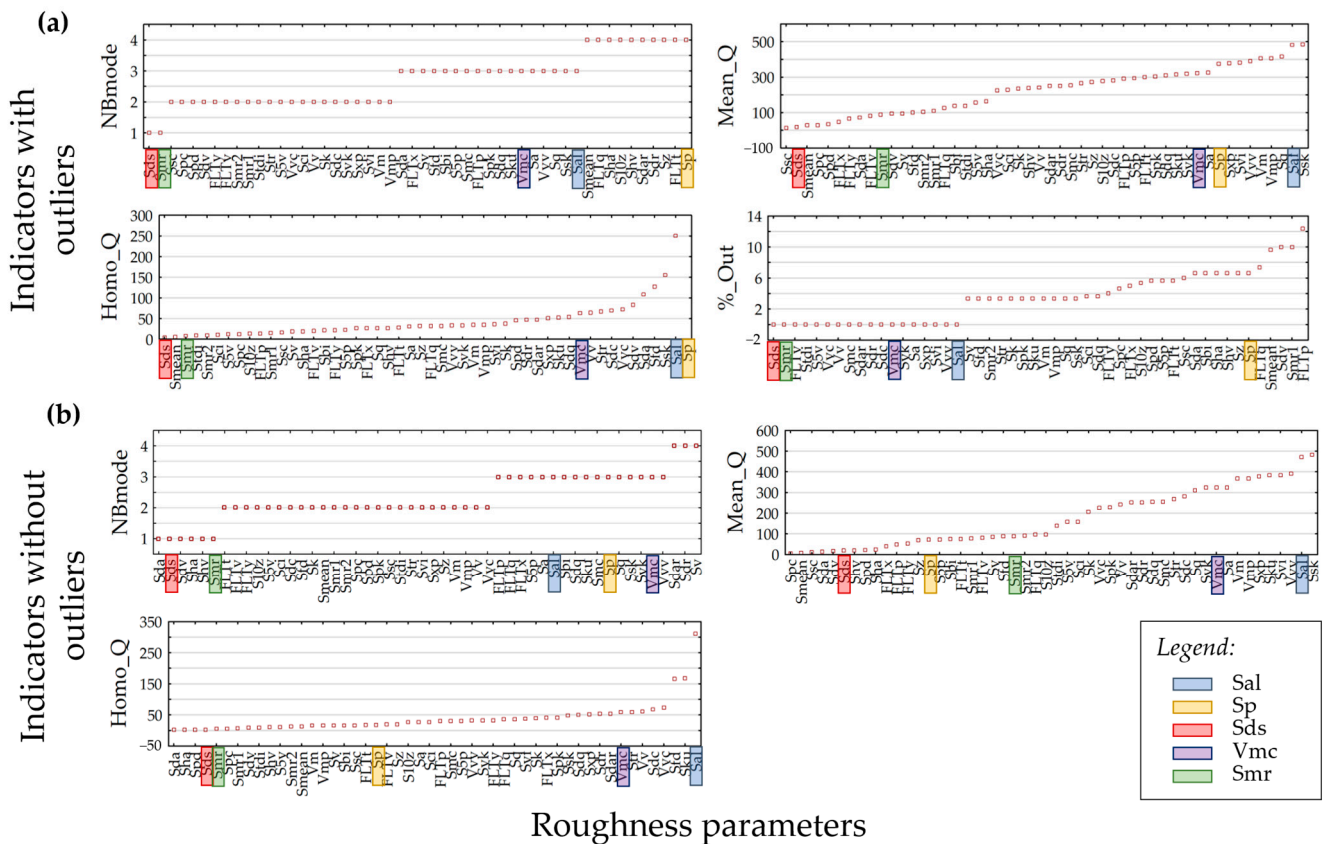*Appendix D.5. Coherence Scanning Interferometry (CSI), Grit #080*

Figure A7. Ranking of the roughness parameters for the indicators (*NBmode*, *Mean_Q*, *Homo_Q*), for the CSI mode and the grit #080: with outliers (**a**) and without outliers (**b**).

Appendix D.6. Coherence Scanning Interferometry (CSI), Grit #120

Figure A8. Ranking of the roughness parameters for the indicators (*NBmode*, *Mean_Q*, *Homo_Q*), for the CSI mode and the grit #120: with outliers (**a**) and without outliers (**b**).

Appendix D.7. Conclusion of Roughness Parameter Ranking

In Figures A3–A8, the parameters Sds, Sp, Vmc, Smr, and Sal are highlighted as examples of application. These parameters were selected based on their performance described in the section 'Results', as either the best or worst roughness parameters, according to the four indicators. It is shown that Sds consistently ranks as the worst parameter in terms of *Mean_Q*, regardless of the instrument mode and grit level. However, Sds does not exhibit a high *%-Out* or a high value of *Homo_Q*, indicating that the raw data are stable and the QI histograms are 'beautiful'. In contrast, Sal is consistently among the best parameters for *Mean_Q*, but it has a high *Homo_Q* value, suggesting poor fitting of the Johnson model to *QI* PDF. This underscores the importance of considering the entire set of indicators. For the Sp roughness parameter, its indicator values show a wide range between the *QI* values computed with and without outliers, due to the high *%-Out*. After removing outliers, Sp does not emerge as the best parameter, demonstrating that data cleaning does not necessarily transform a poor parameter into the best one.

Appendix E. Overview of Roughness Parameters Ranking, Regarding the Severity Rate

The presented results in Figure A9 show the different rankings of roughness parameters depending on the severity rate regarding the instrument modes analysed in the study.
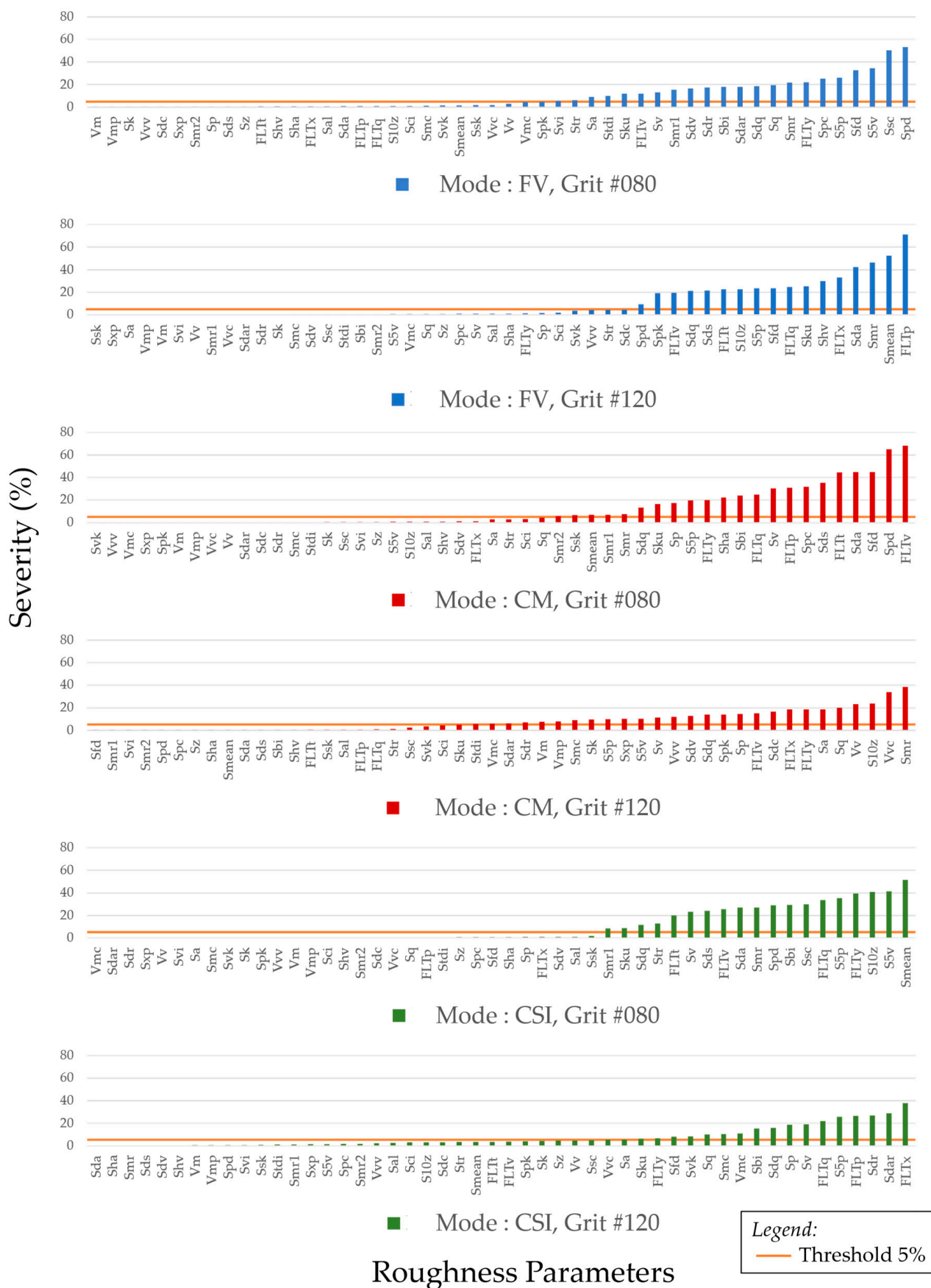
Figure A9. Ranking of roughness parameters from the severity rate for each measurement/grit couple.

References

1. Sun, H.; Wu, X.; Wang, D.; Xu, H.; Liang, X.; Shang, Y. Analysis of Deformation Mechanism of Landslide in Complex Geological Conditions. *Bull. Eng. Geol. Environ.* **2019**, *78*, 4311–4323. [CrossRef]
2. Whitehouse, D.J. Surface Geometry, Miniaturization and Metrology. *Philos. Trans. R. Soc. A Math. Phys. Eng. Sci.* **2012**, *370*, 4042–4065. [CrossRef]
3. Zhao, J.; Tang, J.; Ding, H.; Shao, W.; Zhao, X.; Liu, H.; Jiang, T. A Numerical and Experimental Investigation on the Evolution of Three-Dimensional Surface Topography of 12Cr2Ni4A Steel in Shot Peening. *J. Manuf. Process.* **2021**, *70*, 259–270. [CrossRef]
4. Robbins, S.J.; Watters, W.A.; Chappelow, J.E.; Bray, V.J.; Daubar, I.J.; Craddock, R.A.; Beyer, R.A.; Landis, M.; Ostrach, L.R.; Tornabene, L.; et al. Measuring Impact Crater Depth throughout the Solar System. *Meteorit. Planet. Sci.* **2018**, *53*, 583–637. [CrossRef]
5. Jacobs, T.D.B.; Pastewka, L. Guest Editors Surface Topography as a Material Parameter. *MRS Bull.* **2022**, *47*, 1205–1210. [CrossRef] [PubMed]
6. Ardi, D.T.; Li, Y.G.; Chan, K.H.K.; Blunt, L.; Bache, M.R. Surface Topography and the Impact on Fatigue Performance. *Surf. Topogr. Metrol. Prop.* **2015**, *3*, 015007. [CrossRef]
7. Bagno, A.; Di Bello, C. Surface Treatments and Roughness Properties of Ti-Based Biomaterials. *J. Mater. Sci. Mater. Med.* **2004**, *15*, 935–949. [CrossRef]
8. Bruzzone, A.A.G.; Costa, H.L.; Lonardo, P.M.; Lucca, D.A. Advances in Engineered Surfaces for Functional Performance. *CIRP Ann.* **2008**, *57*, 750–769. [CrossRef]
9. Jiang, X.J.; Whitehouse, D.J. Technological Shifts in Surface Metrology. *CIRP Ann.* **2012**, *61*, 815–836. [CrossRef]
10. Brown, C.A. Surface Metrology Principles for Snow and Ice Friction Studies. *Front. Mech. Eng.* **2021**, *7*, 753906. [CrossRef]
11. Larsen-Badse, J. Influence of Grit Diameter and Specimen Size on Wear during Sliding Abrasion. *Wear* **1968**, *12*, 35–53. [CrossRef]
12. Liu, H.; Liu, H.; Zhu, C.; Parker, R.G. Effects of Lubrication on Gear Performance: A Review. *Mech. Mach. Theory* **2020**, *145*, 103701. [CrossRef]
13. Zhang, H.; Goltsberg, R.; Etsion, I. Modeling Adhesive Wear in Asperity and Rough Surface Contacts: A Review. *Materials* **2022**, *15*, 6855. [CrossRef]
14. Stewart, S.; Ahmed, R. Rolling Contact Fatigue of Surface Coatings—A Review. *Wear* **2002**, *253*, 1132–1144. [CrossRef]
15. Wood, R.J.K.; Lu, P. Coatings and Surface Modification of Alloys for Tribo-Corrosion Applications. *Coatings* **2024**, *14*, 99. [CrossRef]
16. Kumar, S.S.; Hiremath, S.S. Effect of Surface Roughness and Surface Topography on Wettability of Machined Biomaterials Using Flexible Viscoelastic Polymer Abrasive Media. *Surf. Topogr. Metrol. Prop.* **2019**, *7*, 015004. [CrossRef]
17. Królczyk, G.; Kacalak, W.; Wieczorowski, M. 3D Parametric and Nonparametric Description of Surface Topography in Manufacturing Processes. *Materials* **2021**, *14*, 1987. [CrossRef]
18. Kapłonek, W.; Nadolny, K.; Królczyk, G.M. The Use of Focus-Variation Microscopy for the Assessment of Active Surfaces of a New Generation of Coated Abrasive Tools. *Meas. Sci. Rev.* **2016**, *16*, 42–53. [CrossRef]
19. Grochalski, K.; Wieczorowski, M.; H'Roura, J.; Le Goic, G. The Optical Aspect of Errors in Measurements of Surface Asperities Using the Optical Profilometry Method. *Front. Mech. Eng.* **2020**, *6*, 12. [CrossRef]
20. Balcon, M.; Carmignato, S.; Savio, E. Performance Verification of a Confocal Microscope for 3D Metrology Tasks. *Qual. Access Success* **2012**, *13*, 63–66.
21. Schmit, J.; Reed, J.; Novak, E.; Gimzewski, J.K. Performance Advances in Interferometric Optical Profilers for Imaging and Testing. *J. Opt. A Pure Appl. Opt.* **2008**, *10*, 064001. [CrossRef]
22. de Groot, P. Principles of Interference Microscopy for the Measurement of Surface Topography. *Adv. Opt. Photon.* **2015**, *7*, 1. [CrossRef]
23. *JCGM 200*; International Vocabulary of Metrology–Basic and General Concepts and Associated Terms (VIM), 3rd ed. JCGM: Sèvres, France, 2012.
24. Giusca, C.L.; Leach, R.K. *Measurement Good Practice Guide No. 128: Calibration of the Metrological Characteristics of Imaging Confocal Microscopes (ICMs)*; NPL: Teddington, UK, 2012.
25. Giusca, C.L.; Leach, R.K. *Measurement Good Practice Guide No. 127: Calibration of the Metrological Characteristics of Coherence Scanning Interferometers (CSI) and Phase Shifting Interferometers (PSI)*; NPL: Teddington, UK, 2013.
26. Podulka, P. The Effect of Surface Topography Feature Size Density and Distribution on the Results of a Data Processing and Parameters Calculation with a Comparison of Regular Methods. *Materials* **2021**, *14*, 4077. [CrossRef]
27. Aurich, J.C.; Hasse, H. *Component Surfaces: Manufacturing-Morphology-Property Relationships*; Springer Series in Advanced Manufacturing; Springer International Publishing: Cham, Switzerland, 2024; ISBN 978-3-031-35574-5.
28. Lemesle, J.; Guibert, R.; Bigerelle, M. A Novel 3D Topography Stitching Algorithm Based on Reflectance and Multimap. *Appl. Sci.* **2023**, *13*, 857. [CrossRef]
29. Giusca, C.L.; Leach, R.K. Calibration of the Scales of Areal Surface Topography Measuring Instruments: Part 3. Resolution. *Meas. Sci. Technol.* **2013**, *24*, 105010. [CrossRef]
30. De Groot, P.J.; DiSciacca, J. *Surface-Height Measurement Noise in Interference Microscopy*; North Morris, M.B., Creath, K., Burke, J., Davies, A.D., Eds.; SPIE: Bellingham, WA, USA, 2018; p. 26.
31. Saraç, Z.; Groß, R.; Richter, C.; Wiesner, B.; Häusler, G. Optimization of White Light Interferometry on Rough Surfaces Based on Error Analysis. *Optik* **2004**, *115*, 351–357. [CrossRef]

32. *VDI/VDE 2655*; Optical Metrology of Microtopographies—Calibration of Interferometers and Interference Microscopes for form Measurement. VDI Ingenieure: Düsseldorf, Germany, 2020.

33. *JCGM 100*; Evaluation of Measurement Data—Guide to the Expression of Uncertainty in Measurement. JCGM: Sèvres, France, 2008.

34. *JCGM 101*; Guide to the Expression of Uncertainty in Measurement with Supplement 1, Evaluation of Measurement Data. JCGM: Sèvres, France, 2008.

35. *ISO 25178-600*; Geometrical Product Specifications (GPS), Surface Texture: Areal Metrological Characteristics for Areal-Topography Measuring Methods. ISO: Geneva, Switzerland, 2019.

36. *ISO 25178-700*; Geometrical Product Specifications (GPS) Surface Texture: Areal Calibration, Adjustment and Verification of Areal Topography Measuring Instruments. ISO: Geneva, Switzerland, 2022.

37. Pavlíček, P.; Hýbl, O. White-Light Interferometry on Rough Surfaces—Measurement Uncertainty Caused by Noise. *Appl. Opt.* **2012**, *51*, 465. [CrossRef] [PubMed]

38. Pavlíček, P.; Michálek, V. White-Light Interferometry—Envelope Detection by Hilbert Transform and Influence of Noise. *Opt. Lasers Eng.* **2012**, *50*, 1063–1068. [CrossRef]

39. Hering, M.; Körner, K.; Jähne, B. Correlated Speckle Noise in White-Light Interferometry: Theoretical Analysis of Measurement Uncertainty. *Appl. Opt.* **2009**, *48*, 525. [CrossRef]

40. Giusca, C.L.; Leach, R.K.; Helary, F.; Gutauskas, T.; Nimishakavi, L. Calibration of the Scales of Areal Surface Topography-Measuring Instruments: Part 1. Measurement Noise and Residual Flatness. *Meas. Sci. Technol.* **2012**, *23*, 035008. [CrossRef]

41. Giusca, C.L.; Leach, R.K.; Helery, F. Calibration of the Scales of Areal Surface Topography Measuring Instruments: Part 2. Amplification, Linearity and Squareness. *Meas. Sci. Technol.* **2012**, *23*, 065005. [CrossRef]

42. *ISO 25178-6*; Geometrical Product Specifications (GPS). Surface Texture: Areal Classification of Methods for Measuring Surface Texture. ISO: Geneva, Switzerland, 2010; ISBN 978-0-580-70750-6.

43. *ISO 25178-601*; Geometrical Product Specifications (GPS). Surface Texture: Areal Nominal Characteristics of Contact (Stylus) Instruments. ISO: Geneva, Switzerland, 2010; ISBN 978-0-580-60202-3.

44. *ISO 25178-602*; Geometrical Product Specifications (GPS). Surface Texture: Areal Nominal Characteristics of Non-Contact (Confocal Chromatic Probe) Instruments. ISO: Geneva, Switzerland, 2010; ISBN 978-0-580-60203-0.

45. *ISO 25178-603*; Geometrical Product Specifications (GPS). Surface Texture: Areal Nominal Characteristics of Non-Contact (Phase-Shifting Interferometric Microscopy) Instruments. ISO: Geneva, Switzerland, 2013; ISBN 978-0-580-82360-2.

46. *ISO 25178-604*; Geometrical Product Specifications (GPS). Surface Texture: Areal Nominal Characteristics of Non-Contact (Coherence Scanning Interferometry) Instruments. ISO: Geneva, Switzerland, 2013; ISBN 978-0-580-66355-0.

47. *ISO 25178-605*; Geometrical Product Specifications (GPS). Surface Texture: Areal Nominal Characteristics of Non-Contact (Point Autofocus Probe) Instruments. ISO: Geneva, Switzerland, 2014; ISBN 978-0-580-68207-0.

48. *ISO 25178-606*; Geometrical Product Specification (GPS). Surface Texture: Areal Nominal Characteristics of Non-Contact (Focus Variation) Instruments. ISO: Geneva, Switzerland, 2015; ISBN 978-0-580-76436-3.

49. Lemesle, J.; Moreau, C.; Deltombe, R.; Martin, J.; Blateyron, F.; Bigerelle, M.; Brown, C.A. Height Fluctuations and Surface Gradients in Topographic Measurements. *Materials* **2023**, *16*, 5408. [CrossRef] [PubMed]

50. Lemesle, J.; Moreau, C.; Deltombe, R.; Blateyron, F.; Martin, J.; Bigerelle, M.; Brown, C. Top-down Determination of Fluctuations in Topographic Measurements. *Materials* **2023**, *16*, 473. [CrossRef]

51. Vanrusselt, M.; Haitjema, H. Characterization of Measurement and Instrument Noise in Areal Surface Topography Measurements by the Allan Deviation. *CIRP Ann.* **2023**, *72*, 485–488. [CrossRef]

52. Brown, C.A. Uncertainty and Quality in the Measurement and Characterization of the Texture of Abrasive Media. In Proceedings of the ISAAT 2007/SME International Grinding Conference, Dearborn, MI, USA, 26–28 September 2007; Society of Manufacturing Engineers: Dearborn, MI, USA, 2007.

53. Peta, K.; Love, G.; Brown, C.A. Comparing Repeatability and Reproducibility of Topographic Measurement Types Directly Using Linear Regression Analyses of Measured Heights. *Precis. Eng.* **2024**, *88*, 192–203. [CrossRef]

54. Moreau, C.; Bigerelle, M.; Marteau, J.; Lemesle, J.; Paez, D.; Guibert, R.; Blateyron, F.; Brown, C.A. A Novel Methodology to Assess Optical Profilometer Stability to Discriminate Surface Roughness. *Surf. Topogr. Metrol. Prop.* **2024**, *12*, 025018. [CrossRef]

55. Moreau, C.; Lemesle, J.; Páez Margarit, D.; Blateyron, F.; Bigerelle, M. Statistical Analysis of Measurement Processes Using Multi-Physic Instruments: Insights from Stitched Maps. *Metrology* **2024**, *4*, 141–163. [CrossRef]

56. De Groot, P. The Meaning and Measure of Vertical Resolution in Optical Surface Topography Measurement. *Appl. Sci.* **2017**, *7*, 54. [CrossRef]

57. Johnson, N.L. Systems of Frequency Curves Generated by Methods of Translation. *Biometrika* **1949**, *36*, 149–176. [CrossRef]

58. *ISO 25178-1*; Geometrical Product Specifications (GPS)—Surface Texture: Areal—Part 2: Terms, Definitions and Surface Texture Parameters. ISO: Geneva, Switzerland, 2012.

59. Najjar, D.; Bigerelle, M.; Lefebvre, C.; Iost, A. A New Approach to Predict the Pit Depth Extreme Value of a Localized Corrosion Process. *ISIJ Int.* **2003**, *43*, 720–725. [CrossRef]

60. Liu, M.; Cheung, C.F.; Ren, M.; Cheng, C.-H. Estimation of Measurement Uncertainty Caused by Surface Gradient for a White Light Interferometer. *Appl. Opt.* **2015**, *54*, 8670. [CrossRef] [PubMed]

61. Berkmans, F.; Lemesle, J.; Guibert, R.; Wieczorowski, M.; Brown, C.; Bigerelle, M. Two 3D Fractal-Based Approaches for Topographical Characterization: Richardson Patchwork versus Sdr. *Materials* **2024**, *17*, 2386. [CrossRef] [PubMed]
62. Guibert, R.; Hanafi, S.; Deltombe, R.; Bigerelle, M.; Brown, C.A. Comparison of Three Multiscale Methods for Topographic Analyses. *Surf. Topogr. Metrol. Prop.* **2020**, *8*, 024002. [CrossRef]
63. Fu, S.; Cheng, F.; Tjahjowidodo, T. Surface Topography Measurement of Mirror-Finished Surfaces Using Fringe-Patterned Illumination. *Metals* **2020**, *10*, 69. [CrossRef]
64. Jeon, S.H.; Gil, S.-K. Measurement of a Mirror Surface Topography Using 2-Frame Phase-Shifting Digital Interferometry. *J. Opt. Soc. Korea* **2009**, *13*, 245–250. [CrossRef]
65. Leach, R. *Advances in Optical Surface Texture Metrology*; IOP Publishing Ltd.: Bristol, UK, 2020; ISBN 978-0-7503-2528-8.
66. Xue, S.; Chen, S.; Fan, Z.; Zhai, D. Adaptive Wavefront Interferometry for Unknown Free-Form Surfaces. *Opt. Express* **2018**, *26*, 21910. [CrossRef]
67. Mejía-Barbosa, Y.; Malacara-Hernández, D. A Review of Methods for Measuring Corneal Topography. *Optom. Vis. Sci.* **2001**, *78*, 240–253. [CrossRef]
68. Udupa, G.; Singaperumal, M.; Sirohi, R.S.; Kothiyal, M.P. Characterization of Surface Topography by Confocal Microscopy: I. Principles and the Measurement System. *Meas. Sci. Technol.* **2000**, *11*, 305–314. [CrossRef]
69. Feng, X.; Senin, N.; Su, R.; Ramasamy, S.; Leach, R. Optical Measurement of Surface Topographies with Transparent Coatings. *Opt. Lasers Eng.* **2019**, *121*, 261–270. [CrossRef]
70. Leach, R. (Ed.) *Optical Measurement of Surface Topography*; Springer: Berlin/Heidelberg, Germany, 2011; ISBN 978-3-642-12011-4.
71. Bakhtazad, A.; Chowdhury, S. An Evaluation of Optical Profilometry Techniques for CMUT Characterization. *Microsyst. Technol.* **2019**, *25*, 3627–3642. [CrossRef]
72. Jansen, M.; Schellekens, P.; Haitjema, H. Development of a Double Sided Stitching Interferometer for Wafer Characterization. *CIRP Ann.* **2006**, *55*, 555–558. [CrossRef]
73. Gao, F.; Leach, R.K.; Petzing, J.; Coupland, J.M. Surface Measurement Errors Using Commercial Scanning White Light Interferometers. *Meas. Sci. Technol.* **2008**, *19*, 015303. [CrossRef]
74. Su, R.; Wang, Y.; Coupland, J.; Leach, R. On Tilt and Curvature Dependent Errors and the Calibration of Coherence Scanning Interferometry. *Opt. Express* **2017**, *25*, 3297. [CrossRef] [PubMed]
75. Yuan, L.; Guo, T.; Qiu, Z.; Fu, X.; Hu, X. An Analysis of the Focus Variation Microscope and Its Application in the Measurement of Tool Parameter. *Int. J. Precis. Eng. Manuf.* **2020**, *21*, 2249–2261. [CrossRef]
76. Abdel-Aal, H.A.; El Mansori, M.; Mezghani, S. Multi-Scale Investigation of Surface Topography of Ball Python (Python Regius) Shed Skin in Comparison to Human Skin. *Tribol. Lett.* **2010**, *37*, 517–527. [CrossRef]
77. De Groot, P.J. The Instrument Transfer Function for Optical Measurements of Surface Topography. *J. Phys. Photonics* **2021**, *3*, 024004. [CrossRef]
78. Aguilar, J.F.; Méndez, E.R. On the Limitations of the Confocal Scanning Optical Microscope as a Profilometer. *J. Mod. Opt.* **1995**, *42*, 1785–1794. [CrossRef]
79. Mauch, F.; Osten, W. Model-Based Approach for Planning and Evaluation of Confocal Measurements of Rough Surfaces. *Meas. Sci. Technol.* **2014**, *25*, 105002. [CrossRef]
80. Mueller, T.; Jordan, M.; Schneider, T.; Poesch, A.; Reithmeier, E. Measurement of Steep Edges and Undercuts in Confocal Microscopy. *Micron* **2016**, *84*, 79–95. [CrossRef]
81. Senin, N.; Thompson, A.; Leach, R.K. Characterisation of the Topography of Metal Additive Surface Features with Different Measurement Technologies. *Meas. Sci. Technol.* **2017**, *28*, 095003. [CrossRef]
82. Kovalev, A.E.; Dening, K.; Persson, B.N.J.; Gorb, S.N. Surface Topography and Contact Mechanics of Dry and Wet Human Skin. *Beilstein J. Nanotechnol.* **2014**, *5*, 1341–1348. [CrossRef] [PubMed]
83. Marteau, J.; Bigerelle, M.; Mazeran, P.-E.; Bouvier, S. Relation between Roughness and Processing Conditions of AISI 316L Stainless Steel Treated by Ultrasonic Shot Peening. *Tribol. Int.* **2015**, *82*, 319–329. [CrossRef]
84. Pawlus, P.; Reizer, R.; Wieczorowski, M.; Krolczyk, G.M. Study of Surface Texture Measurement Errors. *Measurement* **2023**, *210*, 112568. [CrossRef]
85. Leksycki, K.; Królczyk, J.B. Comparative Assessment of the Surface Topography for Different Optical Profilometry Techniques after Dry Turning of Ti6Al4V Titanium Alloy. *Measurement* **2021**, *169*, 108378. [CrossRef]
86. Masuda, Y.; Oguri, M.; Morinaga, T.; Hirao, T. Three-Dimensional Morphological Characterization of the Skin Surface Micro-Topography Using a Skin Replica and Changes with Age. *Ski. Res. Technol.* **2014**, *20*, 299–306. [CrossRef] [PubMed]
87. Krolczyk, G.M.; Nieslony, P.; Krolczyk, J.B.; Samardzic, I.; Legutko, S.; Hloch, S.; Barrans, S.; Maruda, R.W. Influence of Argon Pollution on the Weld Surface Morphology. *Measurement* **2015**, *70*, 203–213. [CrossRef]
88. Du, J.; Zhang, D.; Wang, X.; Jin, H.; Zhang, W.; Tong, B.; Liu, Y.; Burn, P.L.; Cheng, H.-M.; Ren, W. Extremely Efficient Flexible Organic Solar Cells with a Graphene Transparent Anode: Dependence on Number of Layers and Doping of Graphene. *Carbon* **2021**, *171*, 350–358. [CrossRef]
89. Wei, J.; Li, Y.; Dai, D.; Zhang, F.; Zou, H.; Yang, X.; Ji, Y.; Li, B.; Wei, X. Surface Roughness: A Crucial Factor to Robust Electric Double Layer Capacitors. *ACS Appl. Mater. Interfaces* **2020**, *12*, 5786–5792. [CrossRef]
90. Bigerelle, M.; Mathia, T.; Bouvier, S. The Multi-Scale Roughness Analyses and Modeling of Abrasion with the Grit Size Effect on Ground Surfaces. *Wear* **2012**, *286–287*, 124–135. [CrossRef]

91. Bigerelle, M.; Giljean, S.; Mathia, T.G. Multiscale Characteristic Lengths of Abraded Surfaces: Three Stages of the Grit-Size Effect. *Tribol. Int.* **2011**, *44*, 63–80. [CrossRef]

92. Sasada, T.; Oike, M.; Emori, N. The Effect of Abrasive Grain Size on the Transition between Abrasive and Adhesive Wear. *Wear* **1984**, *97*, 291–302. [CrossRef]

93. Yang, F.; Johnson; Vision, J. Univariate Outlier Detection Using SAS. 2 November 2023. Available online: https://www.wuss.org/proceedings/2023/WUSS-2023-Paper-158.pdf (accessed on 26 October 2024).